An Investigation of Hydroplaning Reduction at Superelevated Highway Transitions in Kansas

By

Adam J.A. Alani
B.S., University of Kansas, 2021

Submitted to the graduate degree program in Civil, Environmental, and Architectural Engineering and the Graduate Faculty of the University of Kansas in partial fulfillment of the requirements for the degree of Master of Science.

_____

Chair: Joshua Roundy, Ph.D.

_____

Alexandra Kondyli, Ph.D.

_____

Steven Schrock, Ph.D.

Date Defended: 9 December 2022

The thesis committee for Adam J.A. Alani certifies that this is the approved version of the following thesis:

An Investigation of Hydroplaning Reduction at Superelevated Highway Transitions in Kansas

Chair: Joshua Roundy, Ph.D.

Alexandra Kondyli, Ph.D.

Steven Schrock, Ph.D.

Date Approved: 12 December 2022

Abstract

Superelevated highway transitions experience an area of zero-cross slope as the outside lane transitions from a normal crown cross slope to superelevation. These areas of poor drainage cause an increase in water accumulation on highways, which can lead to a higher likelihood for hydroplaning and endanger motorists. Across the world, varying weather patterns due to climate change cause stronger precipitation events, which can increase the water on roadways and further exacerbate the potential for hydroplaning along superelevation transitions. Therefore, methods of reducing hydroplaning will become of more importance under a changing climate, yet, identifying areas with increased likelihood of hydroplaning and how to remediate the issue is challenging due to numerous underlying issues that differ from one location to another. To help address this issue, a proactive approach to hydroplaning mitigation is outlined in this study. Several superelevated highway locations with potential hydroplaning problems in Kansas were identified based on expert knowledge from KDOT engineers. These locations were used to identify potential areas of problematic hydroplaning. These potentially problematic locations were then analyzed using data from digital terrain mapping and laser crack measuring systems to pinpoint specific areas near superelevated highway transitions where water would accumulate to induce hydroplaning. Several mitigation strategies are discussed for these locations, including using slope flow path minimization at transition areas to mediate water accumulation issues as well as other methods of mitigating hydroplaning by use of techniques currently used in the United States. Additionally, a robust and broadly applicable method of identifying areas with high wet-weather related crashes was developed by using a general clustering technique along with gridded precipitation data to begin to detect future areas of high hydroplaning potential.

Acknowledgements

I would like to thank my advisor, Dr. Joshua Roundy for his guidance and help through my graduate studies. I've have learned much in his courses involving water resources and hydrology. I am grateful to have had the chance to have worked with him and the brilliant students of his research group. I'd like to thank my professors and committee members Dr. Alexandra Kondyli and Dr. Steven Schrock. Not only have I learned much from them and from their courses involving transportation and highway design, their direction and assistance for finding resources to aid in research was very helpful. I would also like to thank my professors that that have helped me throughout my time at the University of Kansas. Additionally, I would also like to thank those at the Kansas Department of Transportation for providing the funding for this research as well as spending the time to process data requests. Finally, I am extremely grateful for my family and friends for all that they have done for me. Your support was immeasurable.

Table of Contents

List of Figures

List of Tables

Chapter 1: Introduction

1.1 Introduction

The United States is incredibly dependent on roadway transportation systems (Mattioli et al. 2020). Although transportation networks are designed to withstand typical weather, changing weather patterns due to climate show that infrastructure is vulnerable (OECD 2018). As climate change creates more extreme weather events, rainfall intensities will increase (Trenberth 2011). Increase rainfall intensity could impact driver safety if not addressed.

Road crashes due to rainfall are largely caused by the reduction in visibility of the driver, and incidence of dynamic hydroplaning (Ong et al. 2005). Hydroplaning occurs when water build up creates a water film that could provide enough lift to exceed the drainage capacity of a tire tread pattern to the surface of the roadway (AASHTO 2018). Due to this, roadway infrastructure must be reliable during current rainfall events as well as future rainfall intensities (Dong et al. 2017).

As a roadway of normal cross slope heads into a curve, a superelevation transition must occur. In the transition section, there exists an area of the roadway where the cross slope becomes zero and water is slow to drain from the roadway. The geometry at these transitions tends to direct runoff from a large surface area into a smaller cross section, leading to a depth of runoff that may cause hydroplaning.

An important aspect of understanding and mitigating hydroplaning is to model the flow of water due to rain events that flow over superelevated highway transitions. There are many examples of models being used to for this purpose, but many of them are unavailable for industry use. Additionally, the ability to model water film thickness, and thus hydroplaning potential, for highway profiles of complicated design is challenging. Therefore, developing mitigation strategies

for hydroplaning involves many areas of research including hydroplaning mechanics, fluid mechanics, highway design, and material properties.

Given the complicated nature of the problem, this project will focus on the hydraulics and geometry of drainage at curve transitions and will propose methods for predicting where the problem is likely to occur. Secondly, it will list mitigation strategies and then propose recommendations for evaluating potential mitigation strategies. In addition, the study develops a method to identify where a higher likelihood of hydroplaning could occur and identifies ways to mitigate issues based upon rehabilitation and design strategies.

1.2 Superelevated Transitions

To mitigate hydroplaning at superelevated highway transitions, one must understand how the different state departments of transportation throughout the United States design them. The basic components of a superelevated transition are outlined in the AASHTO's "A Policy on Geometric Design of Highways and Streets" (the Green Book) (AASHTO 2018). A superelevated highway transition is the section of roadway where the cross slope of the roadway is superelevated during an alignment transition. An example figure of a superelevation transition is show below from the California Department of Transportation Highway Design Manual (Caltrans 2020).

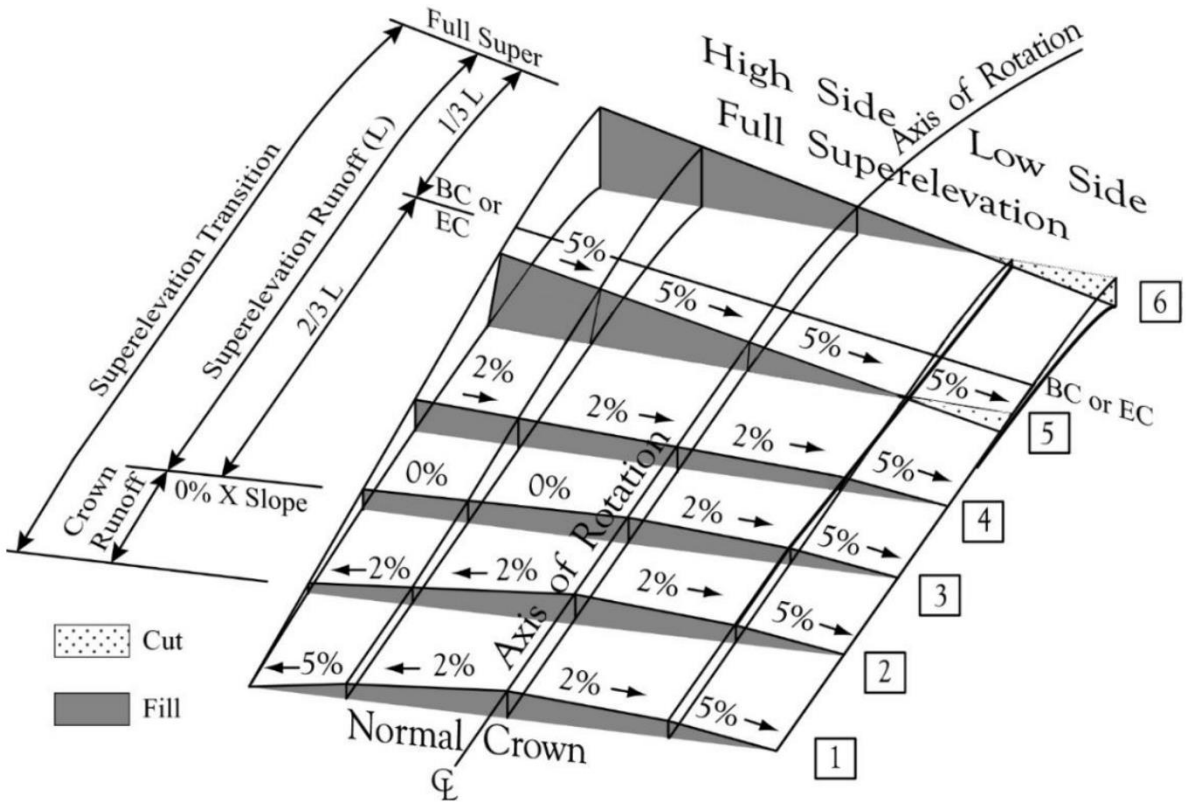

Figure 1: Superelevation transition diagram (Caltrans 2020).

As described by AASHTO in the Green Book (AASHTO 2018), a superelevation transition consists of a superelevation runout and a superelevation runoff. The runout transition is the length needed to transition the outside lane form a normal crown slope to a slope of zero. A runoff transition is the length needed for the outside lane to transition from a cross slope of zero to full superelevation. During this transition, the zero cross slope created leads to lack of drainage from the roadway.

The minimum lengths of the runout and runoff used in a superelevation transition are based on calculations found in the Green Book. The superelevation runoff is based on the width of a traffic lane, the number of rotated lanes, an adjustment factor based on the number of rotated lanes, the design superelevation rate, and the maximum relative gradient. Additionally, the superelevation runout is based on the minimum length of the tangent runout, the normal cross

slope rate, and the design superelevation rate. Section 2.3.4 addresses the runoff and runout lengths. The Kansas DOT recommends using a standard runout length of 75 feet, and also recommends that the desirable slope of edge of pavement profile relative to the profile of the rotation point should not exceed the values shown in the Green Book (KDOT 2014a).

Some state DOTs use spiral curve transitions to smooth the transition from normal cross slope to super elevation. Spiral curves, however, are not addressed in this report. Their use is discouraged in the Kansas DOT highway design manual (KDOT 2014a). Additionally, according to Kansas DOT engineers, spiral curves are not considered for new projects in the state due to their more complicated design and construction.

The Green Book outlines ways transitions can be applied by rotating the lanes of a roadway in Section 3.3.8.6. The first and most common way to create a transition is by rotating the traveled way about the centerline in a normal cross slope scenario. The second way is to rotate the traveled way about its inside edge with a road of normal cross slope. The third way is to rotate the traveled way about the outside edge with a road of normal cross slope. The fourth way is to rotate the traveled way about the outside edge of a road with a straight cross slope.

In order to create a transition, systematic approaches have been developed. Section 3.3.2.3 “Distribution of e and f over a Range of Curves” in the Green Book describes the methods of keeping the vehicle on the roadway when on a lateral curve. This is done by balancing side friction associated with centripetal forces that a vehicle rounding a curve experiences lateral acceleration by the use of roadway superelevation. Engineers create a smooth transition over a distance for driver comfort to avoid abrupt transitions.

AASHTO lays out 5 methods in the Green Book for balancing side friction demand (*f*) with superelevation (*e*) to keep a vehicle on the roadway on a curve. From these methods, Method 5 is

recommended by AASHTO for balancing *e* and *f* for curves with radii greater than the design minimum in rural, freeway, urban, and high-speed street settings. The five methods of accommodating for lateral acceleration on curves using friction demand or superelevation is found below:

"Method 1—Superelevation and side friction are directly proportional to the inverse of the radius (i.e., a straight-line relation exists between $1/R = 0$ and $1/R = 1/R_{min}$).

Method 2—Side friction is such that a vehicle traveling at design speed has all lateral acceleration sustained by side friction on curves up to those designed for f_{max}. For sharper curves, *f* remains equal to f_{max} and superelevation is then used to sustain lateral acceleration until *e* reaches e_{max}. In this method, first *f* and then *e* are increased in inverse proportion to the radius of curvature.

Method 3—Superelevation is such that a vehicle traveling at the design speed has all lateral acceleration sustained by superelevation on curves up to those designed for e_{max}. For sharper curves, *e* remains at e_{max} and side friction is then used to sustain lateral acceleration until *f* reaches f_{max}. In this method, first *e* and then *f* are increased in inverse proportion to the radius of curvature.

Method 4—This method is the same as Method 3, except that it is based on average running speed instead of design speed.

Method 5—Superelevation and side friction are in a curvilinear relation with the inverse of the radius of the curve, with values between those of Methods 1 and 3."

In relation to placing the transition between the tangent and curved section of roadway, Section 3.3.8.2.3 in the Green Book describes where to place this according to the location to the Point of Curvature (PC). To limit lateral acceleration towards outer lanes of traffic, AASHTO prefers to place a portion of the runoff distance before the PC. At the same time, however, too great of the portion of the runoff length on the tangent can create too much negative side friction

from a large superelevation, causing vehicles to drift towards inner lanes of traffic. Most state DOTs use a constant ratio when applying a portion of the runoff length to the tangent. The Green Book cites state DOTs use anywhere from 50 to 80 percent of the tangent length being placed on the tangent with the majority using 67 percent. Highways in Kansas are typically designed with 75 percent of the runoff length being placed before the PC and 25 precent occurring on the circular curve (KDOT 2014a). There is also a check condition in the same section to ensure that the superelevation runoff is placed correctly. If the condition is met, then the transition can be placed with the proportion of runoff to the PC that had been selected.

1.2.1 Green Book Considerations for Superelevated Transitions

To prevent hydroplaning at superelevated transitions, design considerations can be made to mitigate the issue. There are several considerations that AASHTO proposes in the Green Book for highway design at superelevated transitions when considering drainage.

Avoiding placing superelevated transitions at the bottom of a vertical sag curve is one design method to improve drainage. Grade near the transition to the sag curve can be deemed suitable for drainage by using Section 3.3.8.9 in the Green Book. The first technique from this section is to ensure that the minimum profile grade of 0.5 percent is used (or in some cases 0.30 percent). The second technique is to ensure that a minimum of 0.2 percent edge-of-pavement grade for uncurbed sections and a 0.5 percent edge-of-pavement grade is used. It should also be noted that superelevated transition areas that occur on crest vertical curves of low longitudinal grade-in and grade-out slopes can also experience similar, slow drainage issues as seen in sag curves where the longitudinal slope of a crest curve flattens. Additionally, sight distance K-values control the length of vertical curve that can be used.

1.3 Hydroplaning

When considering hydroplaning potential at highway transition areas, hydroplaning mechanics must be considered. There are three different forms of hydroplaning that have been characterized for pneumatic-tired vehicles: dynamic hydroplaning, viscous hydroplaning, and reverted-rubber hydroplaning. Research by Bowne (1975) describes the differences between the types of hydroplaning.

Dynamic hydroplaning occurs when enough fluid is present on a roadway surface to separate the tires of a vehicle from the ground. This case usually occurs when a roadway is flooded. Hydroplaning occurs in this scenario when "the tire exceeds the combined drainage capacity of the tread pattern and the pavement texture… it occurs in deep fluid layers where fluid inertial effects are dominant" (Browne 1975). This area of hydroplaning is the focus for many hydroplaning models and equations, with the other types of hydroplaning not being as widely considered. Only dynamic hydroplaning will be addressed in this report.

Viscous hydroplaning occurs on roadways that are damp with a thin film of water. In this case, the microtexture (with surface depth of less than 0.2 mm) of the roadway is overwhelmed with fluid. Since very small amounts of fluids can cause this form of hydroplaning, it can occur at any speed (Browne 1975).

Reverted-rubber hydroplaning occurs on wet roadways that have less microtexture but where macrotexture (with surface depths of 0.1 to 20 mm) is still present (Browne 1975). In this situation, the wheels of heavy vehicles lock when braking (usually at higher speeds), causing the tire that is contact with the roadway to heat up and begin to melt, triggering the vehicle to lose traction (Browne 1975).

1.3.1 Hydroplaning Characteristics

When enough fluid is present on a roadway, tires of a vehicle can be lifted when the fluid force is equal to or exceeds the vertical force of a vehicle. When the velocity of a vehicle is high enough, tire pressure becomes equivalent to inertial forces of the water film, and the contact patch of the tire and roadway buckles. When this happens, the film of water on the roadway supports the load of the vehicle (Flintsch et al. 2021).

AASHTO describes that "water depth, roadway geometrics, vehicle speed, tire tread design and depth, tire inflation pressure, pavement surface macrotexture, and the condition of the pavement surface" impact hydroplaning (AASHTO 2018). All of these also effect the forces involved with hydroplaning potential. Flintsch et al. (2021) suggests that there are two ways to consider hydroplaning: Fluid lift forces can be compared to the wheel loads, or the vector of the lateral and longitudinal forces can be compared to the force generated by the tire at the operating conditions. In the first situation, wheel loads depend on vehicle characteristics and pavement characteristics. A larger margin between the wheel load and the fluid lift forces allows for improved turning and braking. The second situation describes what forces are available and what forces are needed to prevent hydroplaning.

1.4 Water Film Thickness Models and Equations

When considering hydroplaning at superelevated highway transitions, it is necessary to recognize the methods and equations that estimate hydroplaning speed. Many models and equations for hydroplaning have been developed using water film thickness (WFT) or water film depth (WFD) as input variable. Water film thickness is the height of flowing water over a surface. This WFT for roadways depends on many properties including rainfall intensity, roadway

geometry, roadway drainage, porosity of the pavement, and highway drainage (Flintsch et al. 2021).

There are several methods of calculating WFT, and WFT is often used in equations and models for estimating hydroplaning speed. Many one-dimensional (1D) WFT models have been developed over the years. The 1D models by Gallaway et. al (1971) with TXDOT and the PAVDRN by Anderson et al. (1998) are some of the most widely used models in research and in literature. The model first developed by Gallaway et al. (1971) was later updated to the following equation below by Gallaway et al. (1979). It is an empirical model based on experimentation at test locations.

$$WFT = 0.003726\, MTD^{0.125} L^{0.193} I^{0.562} S^{-0.364} - MTD \quad [1]$$

where WFT is water film thickness (in), MTD is mean texture depth of the pavement (in), L is the length of the drainage path (ft), I is the rainfall intensity (in/h), and S is the cross slope of the roadway (ft/ft). The mean average texture height of the pavement is referred to as the MTD. The PAVDR model is based on the kinetic wave equation. This can be seen in the equation below.

$$WFT = \left(\frac{nLI}{36.1\, S^{0.5}}\right) - MTD \quad [2]$$

where WFT is water film thickness (in), n as the Manning's roughness coefficient (-), L is the length of drainage path (ft), I is the excess rainfall intensity (in/h) or rainfall rate – pavement permeability of the infiltration rate, S is the slope of the drainage path (in/in), and MTD is the mean texture depth of the pavement (in).

More recently, Li et al. (2022) developed a WFT equation specifically for superelevation transitions. The equation from Li et al. (2022) used conservation of mechanical energy while assuming open-channel flow and non-uniform gradient flow. Results showed strong correlation with the Gallaway equation. This can be seen in the equation below where *h* is water depth (m), *v*

is kinematic viscosity at 20 °C (v = 1.003×10^{-6} m^2/s), i is the slope of the flow path (%), g is the gravitational constant (g = 9.8 m^2/s), I is rainfall intensity (m/s), and l is the distance between the starting point and the given section along the flow path (m).

$$h = v^{\frac{1}{12}}\left(\frac{0.3164}{8ig}\right)^{\frac{1}{3}}(Il)^{\frac{7}{12}} \quad [3]$$

Several notable two-dimensional (2D) and three-dimensional (3D) WFT models have also been developed over the years. Ong and Fwa (2007) developed a 3D finite-element model based on mechanics and fluid dynamics. Charbeneau et al. (2008) developed a 2D diffusion wave model specifically for superelevated highway transitions; however, it is not freely available and is therefore unlikely to be utilized by highway engineers. Work by Lottes et al. (2020) and Sitek and Lottes (2020) used computational fluid dynamics to calculate WFT. The results from these studies agreed with the Gallaway for WFT, but the Gallaway model was found to have higher results than the CFD models by Lottes et al. (2020) and Sitek and Lottes (2020) when higher rainfall above six inches per hour when pavement roughness was considered.

1.5 Hydroplaning Models and Equations

As discussed above, there are many models of calculating WFT, and these models have been used to calculate hydroplane speed. Several of the most popular amongst research have been compiled here, including the following:

1. NASA hydroplaning equations developed by Horne and Derher (1963) and expanded on by Horne et al. (1986)
2. Texas DOT equations based on Gallaway et al. (1979)
3. PAVDRN equations based on Anderson et al. (1998)

The NASA equation yields hydroplaning speed based on empirical data. The equation below demonstrates the idea.

$$v_p = 51.80 - 17.15(F_{AR}) + 0.72p \quad [4]$$

where v_p is the hydroplaning speed (mph), F_{AR} is the tire footprint aspect ratio, and p is the tire pressure (psi).

When considering heavy weight vehicles like trucks or trailers, the tire aspect ratio decreases as tire footprint aspect ratio decreases with added weight and is accounted for in the adjusted equation below.

$$v_p = 7.95\sqrt{p(F_{AR})^{-1}} \quad [5]$$

where v_p is the hydroplaning speed (mph), p is the tire pressure (psi), and F_{AR} is the tire footprint aspect ratio. These equations were developed with a WFT of 0.3 in (7.62 mm) assumed, so a WFT is not included as an input parameter.

The Texas equations yield hydroplaning speeds based on empirical data. The relationship was established as

$$v_p = SD^{0.04}p^{0.3}(TD + 1)^{0.06}A \quad [6]$$

where v_p is the hydroplaning speed (mph), $SD = \frac{\omega_d - \omega_w}{\omega_d}\ 100\%$ is the spin down ratio (unitless) and is assumed to be 10%, ω_d is the rotational velocity of the tire on dry pavement (rpm), ω_w is the rotational velocity of the tire on wet pavement (rpm), p is the tire pressure (psi), and TD is the tire tread depth (recommended minimum tread depth is 2/32 in (1.5 mm)) [in 32^{nds} of an inch]. A can be found in the equation below.

$$A = max\left(3.507 + \frac{10.409}{WFT^{0.06}}, \left[\frac{28.952}{WFT^{0.06}} - 7.817\right]T^{0.14}\right) \quad [7]$$

where WFT is the water film thickness (in), and T is the pavement texture depth (in).

The PAVDRN empirical equation can be found below. This model is for use with WFT below 2.4 mm. For WFT above 2.4 mm, the model diverts to using the hydroplaning equation developed by Gallaway et al. for the Texas DOT equations.

$$v_p = 26.04WFT^{-0.259} \quad [8]$$

Shown above, v_p is the hydroplaning speed (mph), and *WFT* is the water film thickness (in).

The Florida DOT adopted a different hydroplaning speed based on research by Gunaratne et al. (2012) that created an analytical solution based on data by Ong and Fwa (2007) to produce a finite-element based fluid model. The resulting equation of the study by Gunaratne et al. can be seen below.

$$v_p = WL^{0.2}p^{0.5}\left(\frac{0.82}{WFT^{0.06}} + 0.49\right) \quad [9]$$

where v_p is the hydroplaning speed (km/h), *WL* is wheel load (N), *p* is tire pressure (kPa), *WFT* is water film thickness (mm).

An equation for trucks was also developed based on the NASA equation and the footprint aspect ratio of a vehicle from the study by Gunaratne et al.

$$v_p = 23.1(p)^{0.21}\left(\frac{1.4}{F_{AR}}\right)^{0.5}\left(\frac{0.268}{WFT^{0.651}} + 1\right) \quad [10]$$

where v_p is the hydroplaning speed (km/h), *p* is tire pressure (kPa), and F_{AR} is the tire footprint aspect ratio, and *WFT* is water film thickness (mm).

An equation for an estimation for the water depth for when hydroplaning would occur at superelevated transitions was also developed by Li et al. (2022). This was done by considering a decrease in friction as it related to lubrication regimes of the roadway due to increases in WFT. A general equation for this can be seen in the equation below where h_t is the hydroplaning threshold water depth, *r* is the tire radius, *N* is the tire load, θ is the resultant gradient of the roadway section, *v* is the velocity of the fluid sheet, *b* is the tire width, and ρ is the density of water.

$$h_t = r - \sqrt{\frac{N^2 cos^2\theta}{v^4 b^2 \rho^2}} \quad [11]$$

The older models of Horne et al. (1986), Gallaway et al. (1979), and Anderson et al. (1998) rely on empirical regression and are not based on mechanics of water flow. Due to this, these models cannot be applied outside the range of the data that was used to generate them (Flintsch et al. 2021).

More recent models, however, are based on physical principals of water flow like diffusion wave and kinematic wave models. These can be better applied to roadway geometry. It has also been noted that kinematic wave models cannot be used near superelevated highway transitions due to the area of the highway where the transition occurs and the roadway slope becomes close to zero (Jeong and Charbeneau 2010). Models using finite element analysis (Noureldin et al. 2006) and computational fluid dynamics (Ong and Fwa 2007) have been created to understand how tire-pavement interactions as well as vehicle dynamics impact hydroplaning. Although models like these are accurate and robust, they are not as readily available for engineering usage (Flintsch et al. 2021), and incorporating these models into the design process is yet to be widespread. Flintsch et al. (2021) did, however, create a design beta version of a tool that focuses on the performance characteristics of different varieties of vehicles using the 1D, WFT equation by Gallaway et al. (1979) that is openly available.

1.6 DOT Design Tools

Tools for roadway slope near superelevated transitions and hydroplaning potential have been created for government DOTs to aid in highway design. The Iowa DOT created an Excel-based tool in 2014 specifically for identifying areas of low slope at superelevated transitions (Iowa DOT 2019). It uses roadway type, runout and runoff lengths, horizontal-curve stationing, vertical curve stationing, vertical point of intersection, back grade, forward grade, and curve length as inputs to find roadway slope near the location of zero cross slope. Using these inputs, the tool

creates a “heatmap” of slope along a map of a highway in a graphical representation. Areas of highway have suitable drainage for the Iowa DOT if resulting slopes are above 0.5 percent. Areas highlighted below this threshold should be reviewed and modified in design. This tool is relatively easy to use, and it is best suited for application to simple highway designs.

In 2012, Florida Department of Transportation (FDOT) developed a hydroplaning prediction tool based in Microsoft’s Excel. In 2020, it was later replaced by another Excel-based tool created by Lee and Ayyala (2020). This multifunction tool calculates WFT predictions on a highway profile of cross slope by lane, lane width, and longitudinal grade. This can be calculated using the tool for a single cross section of a roadway or for a continuously changing length of roadway. WFT can be estimated by the Gallaway (1979) WFT model, U.K. Road Research Laboratory WFT model by Ross and Russam (1968), the modified New Zealand WFT model by Chesterton et al. (2006), and the PAVDRN WFT model by Anderson et al. (1998) and Huebner et al. (1997). The tool then uses these WFT models to estimate a hydroplaning speed based on the Gallaway hydroplaning model by Gallaway et al. (1979), the PAVDRN hydroplaning model by Anderson et al. (1998), and the University of South Florida model mentioned previously by Gunaratne et al. (2012).

A risk analysis using the FDOT tool can be conducted by engineers. Hydroplaning speeds from the models previously discussed can be compared to expected drivers’ speeds based on rainfall using the FDOT tool. Here, research by Jayasooriya and Gunaratne (2014) was used to estimate if a driver will hydroplane on the roadway section during specific rainfall intensities.

A continuous analysis setting allows users to process results for a stretch of roadway with a changing cross slope, grade, pavement texture, or rut depth. Additional support to export a .kml file for use in Google Earth to view results using GPS coordinates is also available.

A probabilistic analysis can also be used with different combinations of input parameters (e.g., rainfall intensity, pavement temperature, axle weight, tire pressure, etc.) using a Monte Carlo simulation to view variations of different variables using a distribution. This would be useful for a user to view likely WFTs and hydroplaning speeds over a distribution of different input parameters.

Although the FDOT hydroplaning tool is beneficial for general hydroplaning estimation, its use for superelevated transition design is limited. As previously mentioned, due to the more complicated geometry of transition areas, more advanced models are needed for WFT and hydroplaning prediction.

1.7 Surface Texture

One of the most common measurements of surface texture is mean texture depth (MTD). MTD is the average macrotexture of a surface and is often found using a volumetric technique like the sand patch method (ASTM 2019). Recently, MTD is also measured using collection vehicles using Multi-Laser Vehicles that collect MTD volumetrically in a digital format (Drenth et al. 2017). When considering the texture of a concrete roadway, the FHWA's Technical Working Group recommended that concrete surfaces have an average MTD of no less than 0.03 inches (0.8 mm) with no individual test result less than 0.02 inches (0.5 mm) (Hibbs and Larson 1996), yet different state agencies have different acceptable MTD values that vary based on pavement application (Snyder 2006). The figure below shows MTD as it is related to WFT.

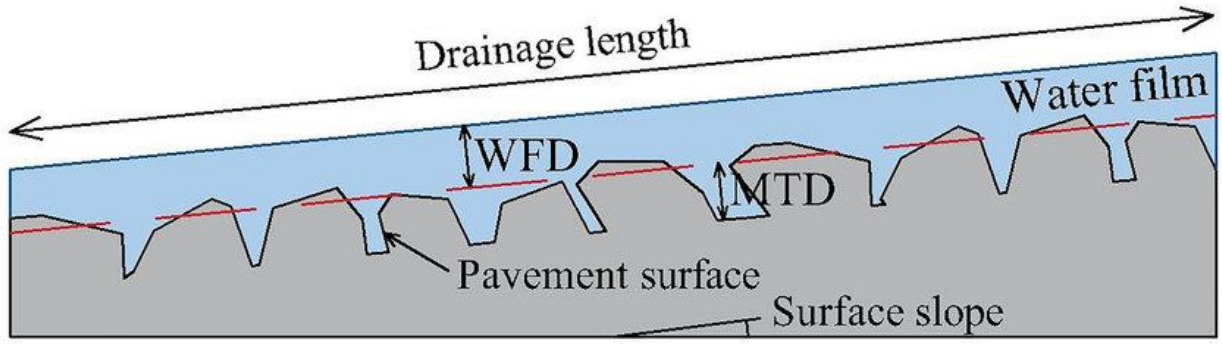

Figure 2: Water film thickness (shown here as WFD), mean texture depth (MTD), and total flow thickness from Pourhassan et al. (2022).

Macrotexture and microtexture are related to the frictional properties of a pavement surface (Kummer and Meyer 1963). Texture depth impacts roadway performance differently depending on heights. Microtexture impacts friction at low speeds while macrotexture has a significant effect on high-speed friction, rolling resistance, and noise (Boulet et al. 1995). Macrotexture also creates porosity on roadway surfaces to increase water drainage and reduce water film thickness (Pranjić and Deluka-Tibljaš 2022).

1.7.1 Roadway Texture and Hydroplaning

High pavement texture is important in hydroplaning scenarios. At areas of high friction demand (like transition areas), pavement can wear quicker leading to a decrease in surface texture (Merritt et al. 2021). Managing texture is important to consider when reducing hydroplaning, especially when considering rehabilitation methods.

Friction on roadways is often quantified as the friction number (FN), where 100 times the force required to slide locked, braking wheels of a trailer over a pavement surface divided by the effective wheel loads is measured (Snyder 2019). The friction number is not directly related to MTD, since it is thought that due to the complexity of the variety of parameters (vehicle speed, aggregate type, roadway moisture, etc.) involved in its measurement, a simple association of the

two is not possible (Zuniga-Garcia and Prozzi 2019). However, it is widely agreed that the primary contributors to pavement performance at high and low vehicle speeds is macrotexture and microtexture (Henry 2000), and that surface texture is the primary property controlling skid resistance to prevent tires from sliding on pavement surfaces (Rajaei et al. 2017).

1.7.2 Pavement Texture and Grooving

There are several techniques of increasing roadway texture. Pavement texturing and grooving is used on concrete and asphalt roadways and can be applied to existing roads or on newly constructed roads. Low-cost treatments used in pavement safety performance can be seen below adapted from Merritt et al. (2015).

Table 1: Flexible and concrete pavement treatment strategies from Merritt et al. (2015).

Flexible Pavement Treatment Strategies	**Concrete Pavement Strategies**
Thin HMA Overlay	Thin HMA Overlay
Open Graded Friction Course (OGFC)	Open Graded Friction Course (OGFC)
Ultra-Thin Bonded Wearing Course (UTBWC)	Ultra-Thin Bonded Wearing Course (UTBWC)
Microsurfacing	Microsurfacing
Shotblasting/Abrading	Shotblasting/Abrading
High Friction Surface Treatment (HFST)	High Friction Surface Treatment (HFST)
Chip Seal (various binder types)	Diamond Grinding
Cape Seal	Grooving
Scrub Seal	Next Generation Concrete Surface
Slurry Seal	
Micro-Milling	

Thin hot mix asphalt (HMA) can be applied to concrete or asphalt pavement to improve friction to a roadway while also correcting minor ruts in the roadway. Open graded friction course is similar to an HMA but uses a porous overlay that allows for added drainage. Ultra-thin bonded wearing courses use an emulsion layer as a binder for asphalt placed on top of concrete or asphalt. Slurry seals use a mixture of emulsified asphalt, water, fine aggregate, and mineral filler that is combined into a slurry and applied to pavement surface in a thin layer. A cape seal is a chip seal

with a slurry seal placed on top. Microsurfacing is similar to a slurry seal, but the binder is modified with a polymer. Shotblasting is when steel pellets are blasted at the roadway surface to add texture (Merritt et al. 2015). All of these measures can improve roadway texture.

Diamond grinding, diamond grooving, and next-generation concrete surfacing are options for existing pavement for increasing MTD by removing top layers of concrete and to texturize roadway surfaces. These are usually applied in the longitudinal direction. Diamond ground surfaces tend to wear quickly compared to other remediation options. Milling and overlays and cross section overbuilds are options for existing roadways. Similar to grinding, milling removes the top layer of pavement and can be used to correct slopes where poor surface drainage occurs. Overlays can be used after milling to also provide a new roadway surface that would correct rutting and poor slope that also contribute to drainage issues (Flintsch et al. 2021).

Rehabilitation techniques differ by location, and even within states. In Kansas, for example, the city of Salina uses microsurfacing, chip sealing, ultra-thin bonded asphalt surfaces, asphalt mills and overlays, diamond grinding, and concrete overlays from the previous discussed solutions (City of Salina 2020), while the city of Lenexa reports using microsurfacing, chip sealing using granite, ultra-thin bonded asphalt surfaces, and mills and overlays from the previous discussed solutions (City of Lenexa n.d.).

Like pavement treatments, pavement grooving and different forms of texture drags can also be used as a means of increasing MTD on roadways. Options like burlap bag drags, turf drags, and broom drags exist for new pavement. Tining, grooving, and exposed aggregate concrete are all options for roadway projects for new pavement and existing pavement. It has been noted that for reducing hydroplaning and increasing drainage, grooves should be parallel to water flow. For maximum effectiveness for hydroplaning reduction and drainage improvement, groves should be

parallel to the slope of the pavement (Flintsch et al., 2021). A comparison of the texture of new pavement and existing pavement restoration can be found in the table below.

Table 2: Typical ranges of macro-texture for new and aged surface textures from Hall et al. (2009).

Texture Type	**Typical MTD for Newly Created Textures, mm**	**Typical MTD for Aged/Trafficked Textures, mm**
New Pavement		
Burlap, Broom, and Standard Turf Drags	0.35 to 0.50	0.30 to 0.45
Heavy Turf Drag	0.50 to 0.90	0.40 to 0.80
Transverse and Transverse Skewed Tine	0.60 to 1.25	0.50 to 1.15
Longitudinal Tine	0.60 to 1.25	0.50 to 1.15
Longitudinal Diamond Grind	0.70 to 1.40	0.50 to 1.25
Longitudinal Grooving	0.80 to 1.50	0.70 to 1.40
EAC	0.90 to 1.60	0.75 to 1.50
Porous PCC	1.20 to 2.50	0.90 to 2.25
Restoration of Existing Pavement		
Longitudinal Diamond Grind	0.70 to 1.40	0.50 to 1.25
Longitudinal Grooving	0.80 to 1.50	0.70 to 1.40
Shotblasted PCC	1.00 to 1.50	0.80 to 1.40
HMA (dense-graded fine)	0.40 to 0.75	0.30 to 0.70
HMA (dense-graded coarse)	0.60 to 1.20	0.50 to 1.10
Ultra-thin Bonded Wearing Course	1.00 to 1.75	0.80 to 1.50

A National Cooperative Highway Research Program report by Hall et al. (2009) contains resources about concrete texturing and their uses in many states in the U.S., including Kansas. Table 3 from Hall et al. (2009) presents concrete pavement surfaces textures along with their benefit ranking.

Table 3: Texture method and ranking by Hall et al. (2009).

Method	**Friction**	**Exterior Noise**	**Cost**	**Constructability**
Transverse tine (0.75-in spacing)	1	8	1	2
Transverse tine (0.5-in. spacing)	1	6	1	2
Transverse tine (variable spacing)	1	7	1	2
Transverse groove	1	7	4	3
Transverse drag	2	6	–	2
Longitudinal tine	1	4	1	1
Longitudinal groove	1	5	3	3
Longitudinal grind	1	3	3	3
Longitudinal burlap drag	4	3	1	1
Longitudinal turf drag	2	3	1	1
Longitudinal plastic brush	3	3	1	1
EAC	2	3	3	4
Shotblasted PCC	1	7	2	3
Porous PCC	1	1	5	4
Ultra-thin epoxied laminate	1	2	6	3
Ultra-thin bonded wearing course	2	2	3	3

Friction and noise relationships become important for selecting the best method of pavement grooving. The texture, friction, and noise associated with the texture methods can also be seen in the table below form Hall et al. (2009).

Table 4: Texture and friction ranges of concrete surfaces by Hall et al. (2009).

Method	Texture Range		Friction Range		Noise Range	
	MTD, mm	**MPD, mm**	**FN40R**	**FN40S**	**CPX, dB (A)**	**CPB L_{max}, dB (A)**
Transverse tine (0.75 in.)	0.53 to 1.1	0.50 to 0.52	41.0 to 56.0	30.6 to 34.4	100.4 to 104.8	83.0 to 84.0
Transverse tine (0.5 in.)		0.35 to 1.00	54.0 to 71.0	37.6 to 62.0		81.9 to 83.0
Transverse tine (variable)	1.14	0.42 to 1.02		50.0 to 69.5		81.0 to 87.3
Transverse groove	1.07			48.0 to 58.0		84.1 to 84.6
Transverse drag	0.76		22.0 to 46.0			
Longitudinal tine	1.22			36.0 to 76.6	96.6 to 103.5	79.0 to 85.0
Longitudinal groove	1.14			48.0 to 55.0	99.4 to 103.8	80.9
Longitudinal grind	0.30 to 1.20		35.0 to 51.0	29.9 to 46.8	95.5 to 102.5	81.2
Longitudinal burlap drag					101.4 to 101.5	
Longitudinal turf drag	0.53 to 1.00		23.0 to 55.6	20.0 to 38.0	97.4 to 98.6	83.7
Longitudinal plastic brush			48.0 to 52.0	23.0 to 24.0	101.8 to 102.2	
EAC	0.9 to 1.1		35.0 to 42.0			
Shot abraded PCC	1.2 to 2.0			34.3 to 46.2		84.3
Porous PCC						
Ultra-thin epoxied laminate	1.4					79.8
Ultra-thin bonded wearing course	0.97 to 1.98		26.0 to 27.0		95.0 to 99.0	

From these methods, Kansas reported that it uses a longitudinal tine of 19 mm (0.75 in) spacing and 3.8 mm (0.15 in) depth with a burlap or a longitudinal turf drag for its texturing of new concrete pavement construction. Kansas also reported locations of longitudinal diamond grinding in Hall et al. (2009). It noted that diamond ground surfaces in Kansas were found to have high friction rankings and can be considered cost-effective replacements to hot mix asphalt resurfacings. This, however, comes with the caveat of higher wheel-to-road noise and micro-texture deterioration due to limestone aggregate use in Kansas.

On roadways, motorcycle riders have stability concerns about the safety of longitudinal and transverse cut tining and groves. A laboratory study by Martinez et al. (1976) tested safety

concerns for motorcycle riders associated with pavement groves of various configurations. Three different motorcycle riders of three different skill levels were test riders. Test riders reported a feeling of uncertainty when riding on longitudinally grooved pavement. Riders had claimed a slight wobble developed at speeds above 70 mph when on longitudinally grooved pavement, but it was concluded that pavement grooving cannot be considered hazardous to riders traveling below 70 mph (except to inexperienced riders). Transverse grooving perpendicular to the direction of travel was not reported to have an impact on riding experience, and riders claimed no discernable difference compared to a roadway with no groves (Martinez et al. 1976).

1.7.3 High Friction Surface Treatments

Unlike other pavement treatment options, high friction surface treatments are used almost exclusively for the safety improvement of pavement (Merritt et al. 2015). “Friction Management in Kansas Department of Transportation Highways” by Zahir et al. (2017) studies how friction can be added to roadway surfaces in Kansas through HFST. HFST is an epoxy or polymer resin binder that is sprayed onto an existing surface with aggregate bonded to the surface that is cured by heat. Aggregate in the treatment layer helps to provide friction on the roadway surface as well as a higher texture depth. These surface treatments can be used in locations where poor roadway geometry or variable superelevations exist. HFST have been used at exit-entrance ramps, horizontal curves, intersections, bridge decks, crosswalks, school crossings, corners, steep grades, bus lanes, roundabouts, toll plazas, and other skid hazard areas. Most states that use HFST end them at the tangent point along a curve. Ride noise, ride quality, and durability remain the same as untreated pavement surfaces.

HFST applied on open-graded friction course or grooved concrete may need two layers of application to create a complete binding to the pavement and create a proper texture depth.

Treatments must be applied to good quality pavements that are clean and dry. Depending on if a hot or cold application method is used, HFSTs can set within 15 minutes to 2 hours respectively. The service lives of these are at least seven years to over ten years of use depending on traffic volumes, traffic type, roadway type, and geometric condition (Merritt et al. 2021). These treatments have a negligible environmental impact, so they don't require long approval periods as they are only applied to road surfaces (Merritt et al. 2021).

During trial applications, states that use HFST's had a 57 to 100 percent decrease in crashes, no matter the weather. Sixty locations in Kentucky saw a crash reduction for dry weather at 85 percent, while wet-weather crashes decreased 78 percent. Based on this and other state DOTs' data, a 20-30 percent reduction in crashes overall and a 50 percent reduction in wet-weather crashes for "general HFS applications" can be expected. A KDOT study of two on-ramps and one off-ramp saw a 20 percent increase of texture depth on asphalt sections and 55 percent increase of texture depth on concrete sections after application with MTD being increased to greater than 1.0 mm. However, the same KDOT study found a decrease in texture depth after a year at a I-70 and northbound K-177 off-ramp location (Zahir et al. 2017).

Implementation of HFST at roadway locations is provided in the Federal Highway Administration guidebook by Merritt et al. (2021). Feasibility, design and field verification, installation, and performance monitoring is also provided in the guidebook.

Chapter 2: Datasets & Methods

2.1 Study Locations

KDOT has indicated that the following highway locations of superelevated transitions have increased hydroplaning potential. They can be found below in the tables and figure below. All annual average daily traffic in this study was taken from state traffic count maps from 2021 (KDOT 2014b). Locations are shown with their mile marker or relative reference point (RP).

Table 5: Study locations in Kansas identified by KDOT engineers.

Location of Interest	Reference Point (RP)	Cardinal Direction of Interest (Northbound, Southbound, Eastbound, Westbound)	Coordinate Location	Annual Average Daily Traffic as of 2021 (Vehicles/Day)
169-2 K-4420-01	79.2	Northbound, Southbound	38.06701, -95.37934	4160
70-84 I-70-3(3)19	204.8	Eastbound	38.84857, -98.48842	13500
35-46 K 9014-01	214.7	Southbound	38.84523, -94.82853	52800
35-46 K 4088-02	217.55	Southbound	38.87682, -94.79362	62900
70-31 K 2611-01	295.2	Eastbound	38.99928, -96.85764	26800
50-9 K 2438-01	330.1	Eastbound, Westbound	38.40531, -96.49143	5180
70-89 K-2446-01	357.7	Westbound	39.06494, -95.73569	57800

Table 6: An extension of Table 5 above with Additional information about the study locations in Kansas.

Reference Point (RP)	Design Speed (mph)	Design Superelevation (%)	Superelevation Rotation Method
79.2	70	1.6 (Rotated Crown)	Center Line
204.8	70	1.5 (Rotated Crown)	Center Line
214.7	70	2.3	Center Line
217.55	70	7.0	Center Line
295.2	70	6.5	Center Line
330.1	60	3.0	Inside Edge
357.7	65	4.1	Outside Edge

Table 7: An extension of Table 6 above with additional information about the study locations in Kansas.

Location Reference Point (RP)	**Transition Runout Length (ft)**	**Transition Runoff Length (ft)**	**Horizontal Curve Length (ft)**	**Horizontal Curve Radius (ft)**
79.2	75	200	6484.99	11459.16
204.8	75	150	1200	17188.76
214.7	23	91	339.35	2772.77
217.55	284	840	1421.53	2864.79
295.2	75	275	2864.79	1655.5
330.1	75	175	2703.33	5729.63
357.7	25	275	338.57	3819.72

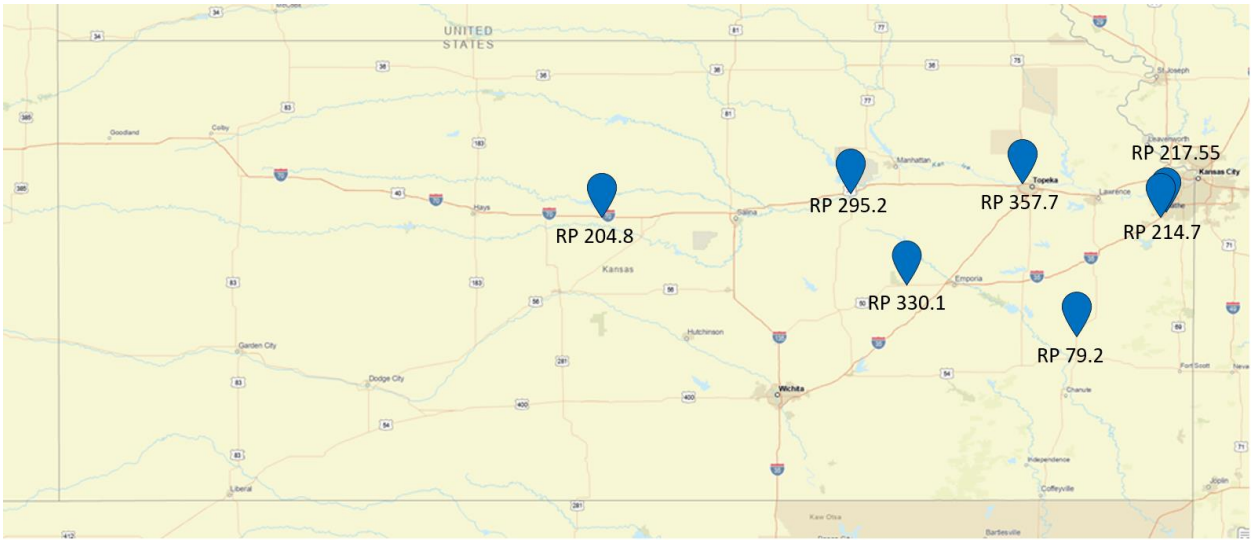

Figure 3: Map of study locations in Kansas (show in blue markers).

Approximate locations of the superelevated transitions in each study location based on design drawings are included in the figures below, where a yellow line designates the beginning of the runoff length, a partial red line designates the location of the zero-cross slope (the beginning of the runout length), and a green line represents the end of the runout length as the curve

transitions into full superelevation. The coordinate location given for each of the study locations is marked with a red pin.

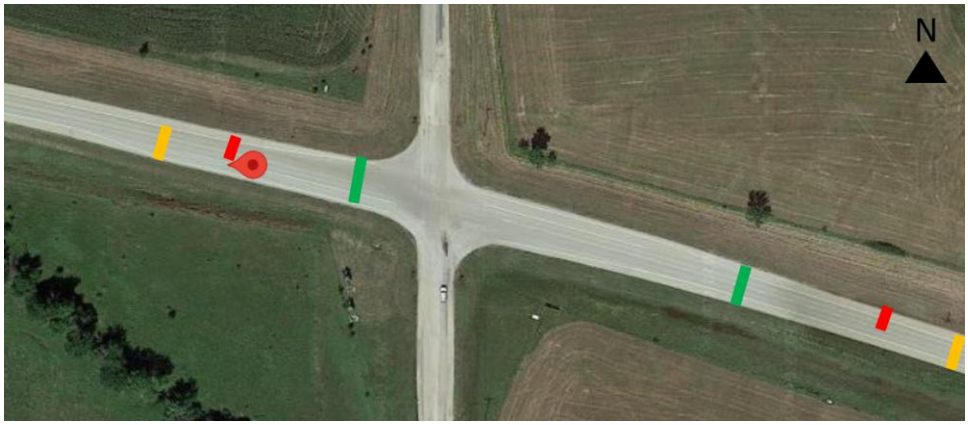

Figure 4: Approximated superelevated transitions at RP 79.2.

The RP 79.2 location is near a crest curve of 800 ft that peaks at an intersection. The entirety of intersection in the direction of interest is superelevated. This location uses a rotated crown superelevation. The longitudinal grade-in from the south is +1.02 percent and the grade out to the north of the intersection is -0.4 percent.

Figure 5: Approximated superelevated transitions at RP 204.8.

The location at RP 204.8 has sag curve of 600 feet that occurs near the transition area east of the marker where the longitudinal grade-in is -0.78 percent and the grade-out +0.98 percent. At the RP 214.7 location the inner lane of the site superelevates causing the zero-cross slope to occur at the median barrier, and cross slope to drain into the inside lane. There is only one median drain

at the zero-cross slope at this location within 200 feet in either direction, which could lead to drainage problems. The bottom of a sag curve occurs after the section reaches full superelevation.

Figure 6: Approximated superelevated transitions at RP 217.55.

Figure 7: Approximated superelevated transitions at RP 214.7.

Similarly, to the RP 214.7 location, the RP 217.55 location also experiences a zero-cross slope at the inside lane by the median barrier. This area, however, does have more median drainage than the former. A large sag curve occurs about 200 feet from the beginning of the superelevation transition.

Figure 8: Approximated superelevated transitions at RP 295.2.

The on-ramp acceleration lane of RP 295.2 location (Figure 8) occurs at the zero-cross slope. The end of the acceleration lane taper ends as the curve transitions to full superelevation. Traffic travels downhill in this location.

Figure 9: Approximated superelevated transitions at RP 330.1.

The location at RP 330.1 (Figure 9) is a location of a 600 ft sag curve that occurs at the location of the marker where a stream flows under the roadway. The longitudinal slope heading into the curve is -0.60 percent while the slope exiting the curve is +3.60 percent.

The location at RP 357.7 is a cross-over weave where the superelevation transition occurs over a short distance. This area transitions from full superelevation that slopes to the outside weave lanes and ends with a cross sloping to the median. This location has two drains on the weave itself and another drain between where the zero-cross slope occurs and where full superelevation is reached.

Figure 10: Approximated superelevated transitions at RP 357.7.

2.1.1 Site Visits

Locations near RP 217.55, RP 214.7, RP 357.7, RP 295.2, and RP 330.1 were all visited to gain a better understanding of each of them. Site visits confirmed that each location had factors that would lead to drainage issues and subsequent possible hydroplaning.

At the location near RP 214.7, headed southbound, the roadway geometry could very well could cause drivers to hydroplane. A gore area next to Exit 214 at this location also attributes to a larger contribution area that could also increase the amount of flow that the exit lane experiences during rain events. Lower slopes that would drain flow to the right of the roadway and flow down the ramp could potentially occur at this location.

Figure 11: Gore area facing southbound direction near RP 214.7.

At the location near RP 217.55 heading southbound, is the location of a high water table. Groundwater at this location could rise high enough for water to inundate low-lying roadway areas to cause hydroplaning. Correcting the hydroplaning problem experienced at this location may be associated more with eliminating water seepage due to groundwater rather than an issue of correcting the superelevated transition. A more thorough investigation of the location would need

to take place to determined which issue has a larger impact on hydroplaning at this location. Images of this location are included below.

Figure 13: Dampness shown facing southbound direction near RP 217.55.

Figure 12: Facing northbound direction near RP 217.55.

Figure 14: Washout near guardrail near RP 217.55.

At the location near RP 295.2 headed eastbound, traffic heads downhill towards a horizontal curve. An onramp is also located right before the curve. Flow traveling downhill in the

direction of traffic could have hydroplaning potential. Around the area of the cross-over was the pointed location of the high sheet flow. Images of this location are included below.

Figure 15: Facing eastbound direction near RP 295.2.

Figure 16: Facing westbound direction near RP 295.2.

The RP 330.1 location features a culvert that travels underneath the area, but this appears to not have an impact on drainage of the roadway surface, as the roadway itself is elevated far above the culvert area. This reference point is the location of a sag curve with a large attenuation area from both the east and westbound directions. The shoulder of the lane headed in the westbound direction, by the guardrail, was discolored compared to the rest of the location. This appeared to be an area of a surface milling project to attempt to possibly correct poor drainage due to geometry. There could also be decreased roadway friction at this location due to normal use or poor drainage over time. Figures showing the east and westbound directions near RP 330.1 can be seen below.

Figure 18: Facing eastbound direction near RP 330.1.

Figure 17: Facing westbound direction near RP 330.1.

At the location near RP 357.7 headed westbound, roadway geometry appears to be the main cause of the hydroplaning experienced by drivers. Near Exit 357B at this location, the roadway slope is the opposite direction of the flow of traffic. It has been reported that during rain events, flow is funneled towards traffic. As vehicles move uphill, they spray water back uphill with the direction of traffic. This causes accumulation of flow traveling downhill and against traffic. During higher rainfall, hydroplaning potential increases in this area. Images of this location are included below.

Figure 19: Facing southbound direction near RP 357.7.

Figure 20: Facing northbound direction near RP 357.7.

2.2 Datasets

After investigating and photographing study locations, subsequent conversations with KDOT engineers were initiated. Design plans of highway segments did not resemble the as-built locations and conditions pictured. This proves that accurate highway profiles are needed to understand cross-slope for proper drainage.

There are several methods of creating highway profiles for as-built infrastructure, and each has a different combination of safety for collection, cost, time-consumption for measurement, and accuracy. Conventional surveying of a location can be conducted, but this can be time-consuming, sometimes requires road closures, and most importantly, puts surveying crews in close proximity to road traffic (Souleyrette et al. 2003). Stereo photography is accurate, but time consuming, and expensive. Mobile laser scanning (MLS) could be of use for this application. When data collection

when using MLS is conducted, many lanes of data can be collected in a single pass at highway speeds by a vehicle with collection equipment (Shams et al. 2018).

The KDOT Mobile LiDAR Project was used as a data source to create accurate highway profiles. KDOT collected Light Detection and Ranging (LiDAR) data for much of the Kansas state highway system from March 2021 to April 2021 (KDOT 2022). Data that can be requested from this project include LiDAR files and Laser Crack Measuring System (LCMS) data. Although the KDOT Mobile LiDAR Project was conducted primarily with roadway asset collection (KDOT 2022), previous studies have shown that LiDAR data can be used to create roadway profiles. Studies conducted by Zhang and Frey (2006), Tsai et al. (2013), Holgado-Barco et al. (2014), and Shams et al. (2018) have shown that using mobile LiDAR is an accurate and effective method for measuring highway cross-slope. Notably, research by Gurganusa et al. (2021) evaluated areas on highways that were identified as having hydroplaning speeds below posted speed limits using mobile LiDAR to delineate basins on the road.

In addition to roadway scanning and mapping, design plans for the study locations as well as crash data for the entire highway system of Kansas was used. Highway design plan sheets for the study locations included typical sections, horizontal, and vertical alignment of the locations and their superelevation transitions. Crash data for the entire state was also used, in addition to what was requested for the study locations.

2.2.1 Digital Terrain Mapping

Data from the LDTM scanners creates a 3D point cloud using laser line projectors (“Pavemetrics | Laser Digital Terrain Mapping System (LDTM)” n.d.). As the collection vehicle travels down the roadway at highway speed, it captures the surface of the roadway and the surrounding area. The LDTM data from the LiDAR project was collected using a Pavemetrics

Laser Digital Terrain Mapping System (LDTM). The LMDT scanner collects 112 million data points per second, and it has a vertical accuracy of +/- 3 mm and has a 1 sigma standard deviation for straight and curved roadways ("Pavemetrics | Laser Digital Terrain Mapping System (LDTM)" n.d.). This data identified specific areas of study locations where flow was likely to accumulate and the directions on the roadway where flow was likely to drain to.

2.2.2 Laser Crack Measuring System Data

Similarly to LDTM, LCMS data is collected by using laser line projectors using an array of scanners to create a profile of the roadway ("Pavemetrics | Laser Crack Measurement System (LCMS)" n.d.). Data from the LCMS was collected using a Pavemetrics Laser Crack Measurement System (LCMS-2) that has a transversal resolution of 1 mm over a width a 4 m, a vertical accuracy of 0.25 mm, and a vertical resolution of 0.05 mm at a 95 percent confidence interval ("Pavemetrics | Laser Crack Measurement System (LCMS)" n.d.).

2.2.3 State Crash Data

In order to understand hydroplaning across the state of Kansas, and specifically at the study locations, crash data from KDOT was requested for the entire state using public data reports to evaluate areas of wet-weather related crashes (KDOT 2017, 2022). Data involved all crashes on Kansas highways from January 1, 2011, to December 31, 2021, in urban and rural areas. Information such as dates, times, coordinate locations, crash locations on the road (shoulder, intersection, etc.), directions of travel, type of crashes, mechanism of crashes, vehicles involved, weather types, and lighting conditions was among the data that was included in the crash reports. Location data of crashes are reported using smartphone GPS accurate within 10 ft (KDOT 2019).

2.3 Methods

Different methods were used when considering the analysis data. State crash data was used for identifying crashes at the study locations as well as identifying clusters of crashes at a state level related to wet-weather crashes. ArcGIS Pro ("ArcGIS Pro" 2022) was used to evaluate flow direction and flow accumulation at each of the areas of concern. OpenRoads Designer ("OpenRoads Designer" 2022) was used to identify areas of long flow path in an example highway design by using slope length. Each of these methods are discussed in greater detail below.

2.3.1 Identifying Locations of High Wet-Weather Crash Frequency

To identify areas where there was a high likelihood for hydroplaning at superelevated highway transitions, areas with a high frequency of wet-weather related crashes were considered by using crash data obtained for the state of Kansas. These areas can be preemptively identified when considering potential increases in wet-weather related crashes due to more intense storm events (Trenberth 2011).

Due to lack of parameters like free flow time, congested flow time, roadway section length, assigned traffic volumes to roadway sections, and isolating crashes to urban and rural settings, it was not feasible to perform a more in-depth analysis of crash clusters using techniques like kernel density estimation (Ledl 2004), KLINGS method (Yamada and Thill 2004), or Local Moran's I statistic (Anselin 1995). A general method of identifying hazardous road locations using proximity by cluster grouping was used.

Clusters were created by first selecting a crash as a starting cluster and then a second crash is selected. This second crash is checked if it is within a distance threshold. In this case, distances of 500 m (1640.42 ft), 1000 m (3280.84 ft), and 1500 m (4921.26 ft) were compared as a threshold distance. If the second selected crash is within the threshold, then the crash is added to the cluster.

The position of the cluster is then updated to the average latitude and longitude coordinates for all crashes in the cluster. If the selected crash is outside the threshold of all existing clusters, then a new cluster is created. This process is repeated for all 224,282 crashes over the analyzed time frame. Clusters with over sixty percent of the crashes occurring during wet weather were then identified by using a gridded precipitation product.

The North American Land Data Assimilation System (NLDAS) data set ("NLDAS: Project Goals" 2022) was used to evaluate precipitation at the time of the crash. NLDAS is a reanalysis data set that is derived from the North American Regional Reanalysis (NARR) (Xia et al. 2012). Precipitation data was used from this data set. NLDAS has a spatial resolution of 12 km and an hourly timestep. A timespan of +/- 2 hours from the time of the crash was used to identify if precipitation had occurred during a crash in order to minimize inaccuracies associated with the time that a crash was reported.

2.3.2 Hydroplaning Remediation Approach

Once a cluster of high wet-weather crashes is identified, systematic approaches should be used when considering remediation efforts at transition areas that experience hydroplaning. Cost should be considered when choosing appropriate solutions to maximize benefit. Remediation strategies can be separated into two categories: correcting areas experiencing poor drainage and correcting areas of poor friction. Areas of poor drainage can be identified on roadways using flow direction and accumulation models alongside examining cross slopes and longitudinal slopes. Areas of poor texture can be found using MTD on roadway sections. Within these areas is overlap that both help solve poor drainage and low texture problems. The table below is an example of workable solutions to both problem areas.

Table 8: Methods of remediating hydroplaning.

Poor Drainage Remediation and Poor Texture Remediation	
Overlay and overbuild	
Surface tining or grove cutting	
Milling or diamond grinding	
Seals, bonds, and resurfacing	
Poor Drainage Remediation	**Poor Texture Remediation**
Permeable pavements	High friction surface treatments
Geometry redesign (adjust slopes or configuration adjustment)	
Drainage redesign (adding additional drainage)	

Although included here for poor draining areas, permeable pavements would not be recommended for use in Kansas due to harsh winters. However, these solutions do allow for water to flow through them, lowering the WFT on the roadway (Bill et al. 2007). A more extreme mitigation strategy is to redesign the roadway to improve drainage and is usually only considered as a final course of action when other correction methods are not applicable. The main reason for this is that highway geometric redesign projects are costly, however, in order to achieve maximum effectiveness from pavement treatment, proper highway geometry is needed (Merritt et al. 2015).

2.3.2 Flow Direction and Flow Accumulation

Digital terrain mapping was used for flow direction and accumulation inspection on the superelevated transitions of the study areas in order to recommend remediation efforts. Data was delivered in a zipped LAZ LiDAR file type. LASTools ("LAStools" 2021) was utilized to convert LAZ files to a LAS file type to be loaded into software to model the data in 3D. Scale of the LAS scans and georeferenced metadata of points within the LAS data was not available.

Although the scale of the LAS data and its georeferenced location could not be changed or verified, location and scale are not necessary for qualitative flow direction and flow accumulation applications based off slope. All LAS data was processed using ArcGIS Pro. ArcGIS Pro was used to filter out noise to isolate the roadway surface and the ground. A digital elevation model (DEM)

of the roadway was then created using the “LAS Dataset to Raster” in ArcGIS Pro. Interpolation was set to binning, cell assignment was set to average, and a linear void filling method was used. A sampling value of 0.01 was used. This was found to preserve the accuracy of the 3D scan, but not compromise processing time. The z factor remained unchanged.

Once a DEM of the study areas had been created, the roadway surface was isolated. The isolated roadway DEM was pit filled, using no z limit. This was necessary to avoid indeterminant flow that would cause processing issues for resampling. Flow direction and flow accumulation of the roadway can then be considered. Flow direction was found using the D8 method, where edges were not forced to flow outward. Directional arrows were placed on top of the flow direction based on the results of the D8 method. A flow accumulation was then performed to identify areas of the roadway where flow drainage stagnated and where it was likely to collect. The resulting flow direction and flow accumulation rasters were upscaled to a rectangular cell size of 0.05 by 0.05 using the majority of the value that occurred most often of the cells in a cell block.

2.3.3 Roadway Texture and Slopes

LCMS data received from the KDOT LiDAR project showed that systems took five different scans along the roadway at a single interval with location coordinate data for each scan in according to the five standard AASHTO scanning bans of the center, right and left wheel paths and outside section of roadway (Laurent et al. 2008). Various data points were collected at each interval, including MTD, cross slope, longitudinal slope, latitude, and longitude coordinates. MTD and cross slope at each interval was averaged, as well as the coordinates of each scan to yield an average location, MTD, and cross slope for the interval. Only one longitudinal slope was given per scan interval. Scan intervals were plotted, and the locations of each interval were numbered along a map of the roadway to track changes over distance and into transition areas.

2.3.4 Highway Redesign Using Slope-Path Length

If a redesign of a highway section is necessary, resulting options are dependent on current design factors and goals. Design solutions are weighed with road surface drainage efficiency as well as cost effectiveness. Solutions for a geometric redesign of a highway transition to mitigate hydroplaning will vary based on the highway section being considered.

From the problem locations indicated by KDOT, the site at RP 295.4 was selected as an example location for a geometric redesign. This area was selected due to findings of high water accumulation near the superelevation transition. This location is also based on an original design from 1989, meaning design revisions could be made based on more recent design practices. In the eastbound direction, the RP 295.4 location also has an acceleration lane near the transition experiencing hydroplaning reports. Further investigation was conducted to see if the acceleration ramp lane contributed to increased hydroplaning likelihood. An aerial view of the location can be seen in the figure below.

Figure 21: RP 295.4 location with superelevated transition noted.

The highway section at RP 295.4 has a design speed of 70 mph and traffic flows in an eastbound direction. This segment features 12-foot-wide lanes, with an inside shoulder width of 6 feet, an outside shoulder width of 10 feet, and an outside shoulder width of 8 feet at the acceleration lane. The acceleration lane has a design speed of 30 mph, as this was the same design speed used

for the other ramps at the interchange for this section. This section features a parallel-type entrance, an entrance ramp radius of 1432.39 feet, a parallel acceleration lane entrance length of 810.00 feet (measured from where right edge of the traveled way of the ramp joins the traveled way of the freeway to the beginning of the acceleration lane taper), and a taper ramp length of 300.00 feet. The superelevated highway transition occurs near where the acceleration lane taper begins, with full superelevation of 6.5 percent being achieved in the outermost lane near the end of the taper.

In the direction of road travel, the longitudinal slope is -2.66 percent. A sag curve occurs about 160 feet from the end of the superelevation transition, where the longitudinal slope shifts from -2.66 to -0.05 percent. The transition meets design criteria of the May 2014 edition of the KDOT highway design manual. Given the 2864.79-foot radius of horizontal curve, an e_{max} of 8.0 percent was used. A runout length of 75 feet and a runoff length of 275 feet was used at this location, with 75 percent of the runoff distance occurring before the PC.

The cross slope of the acceleration lane slopes in the same direction as the right through lane for proper drainage, but this creates a drainage issue when the acceleration lane tapers to an end just as it must match the cross slope as the right lane heads into a superelevation transition. The roadway design specifications of the section were acquired and were reproduced in OpenRoad Designer (ORD) software in 3D. ORD was selected because it is a highway design tool that is used by many state departments of transportation. Examples of the completed corridor section in ORD can be seen below.

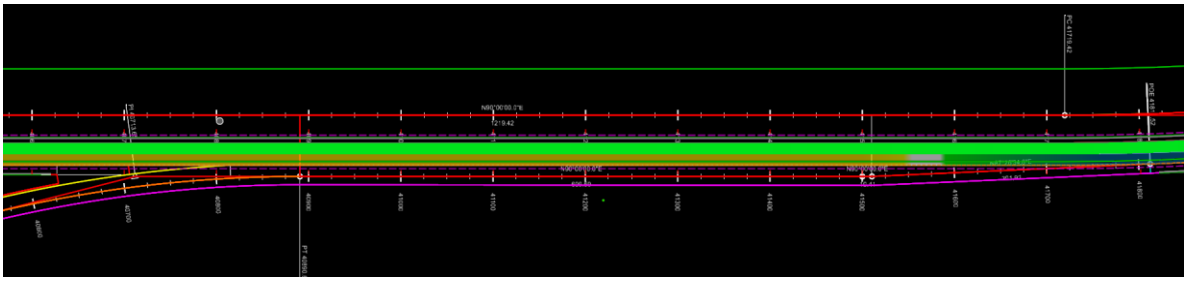

Figure 22: Horizontal alignment of RP 295.4 location in ORD.

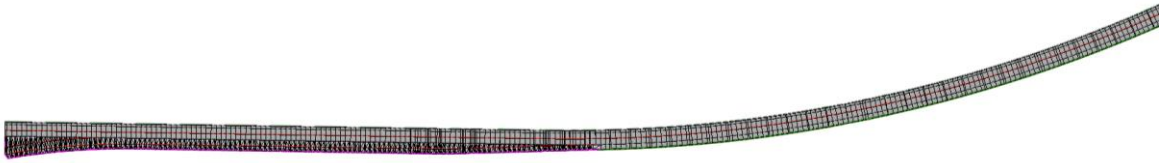

Figure 23: 3D corridor model of RP 295.4 location in ORD.

The roadway was made by first creating a horizontal alignment and assigning a vertical alignment to the section. A corridor template was made for the section and added to the alignment at an interval of 10 feet. The 10-foot interval was chosen to be able to identify areas of poor drainage with reasonable accuracy. For design of the on-ramp, variable slope offsets were applied to cross-sections of the ramp to project the elements in 3D space. A terrain mesh of the roadway was created by selecting the handles of each road element to create an accurate roadway surface.

The superelevation transition of the section can be seen in the figure below, where the right lane transitions to a zero slope as the taper of the acceleration lane begins. According to the design plans, the traveled way is revolved about the centerline profile.

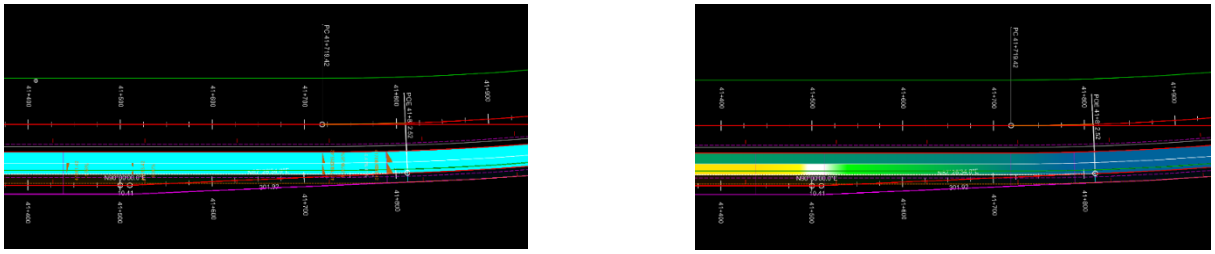

Figure 24: Superelevation transition of RP 295.4 location in ORD where cross slope change can be seen in the lanes of the left panel and visually this can be exhibited in the panel on the right where the right lane transitions from yellow to green.

The right lane is shown with a heatmap (Figure 24, right panel) of where the transition occurs. This can be seen in the figure above where the yellow lane transitions to white and then to green before the horizontal curve.

Using this ORD model, several geometric redesigns were developed for the selected location. These redesigns focus on relatively simple changes and are meant to provide examples of possible solutions. The examples do not constitute an exhaustive set of solutions for either this location or all study locations. Therefore, it is recommended that site specific potential design solutions be consider that maximize draining performance.

Chapter 3: Results

3.1 Site Assessment for Hydroplaning

Hydroplaning at each KDOT identified location is analyzed for hydroplaning potential through a series of analysis that considers MTD, cross slope, longitudinal slope, and flow direction and accumulation. Results from using the laser crack measurements and digital terrain mapping for quantifying the potential risk of hydroplaning based on MTD, flow direction and accumulation are given for each location in the sections below, followed by a summary of the overall hydroplaning potential and mitigation strategies at each location. Intervals are labeled along the roadway sections where MTD and slopes were measured. Arrows present flow direction by the D8 method, and flow accumulation is given by the colormap where green indicates low accumulation and red indicates high accumulation. This analysis is broken up into sections based off of each KDOT identified location.

3.1.1 RP 79.2 Results

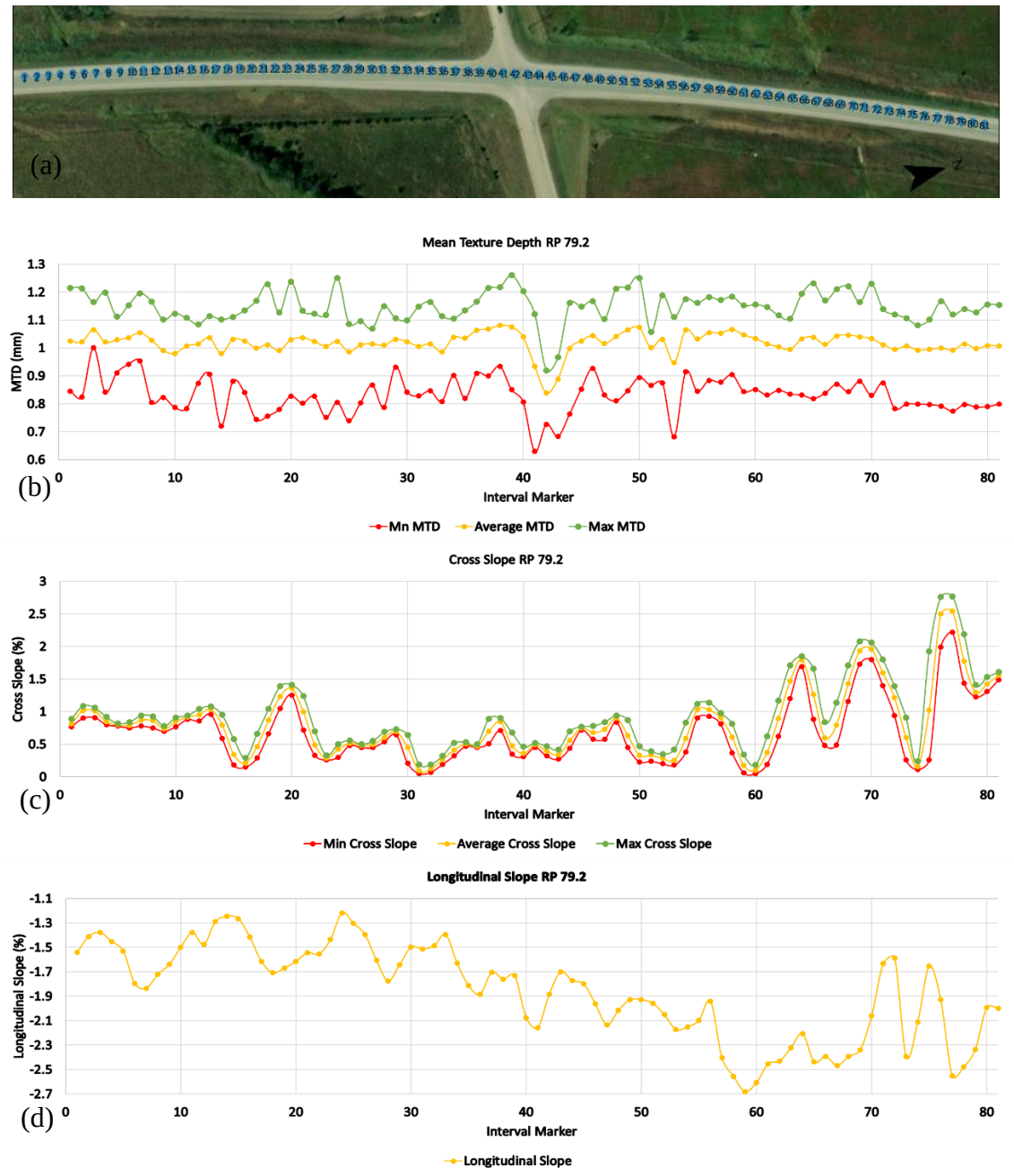

Figure 25: Scan locations (a), MTD (b), cross slope (c), and longitudinal slope (d) for RP 79.2 section.

Figure 26: Flow direction (a) and flow accumulation (b) for RP 79.2 section.

When looking at the MTD of the RP 79.2 location, a dip can be seen near the intersection where cross slope and longitudinal slope begin to decrease. Considering vehicles travel in all directions at the intersection, this decrease in texture is not unexpected. Minimum MTD for this location begins to dip below 0.8 mm at the superelevated transitions. The average MTD of the section of 1.1 mm, and the lowest MTD being 0.6. Flow accumulation can be seen in the turning lane traveling north with the highest accumulation seen near the transition of the north end of the section. Flow direction is seen traveling nearly in the same direction as traffic on the south end of the section. With an adequate roadway MTD, a drainage improvement can be recommended at this location.

3.1.2 RP 204.8 Results

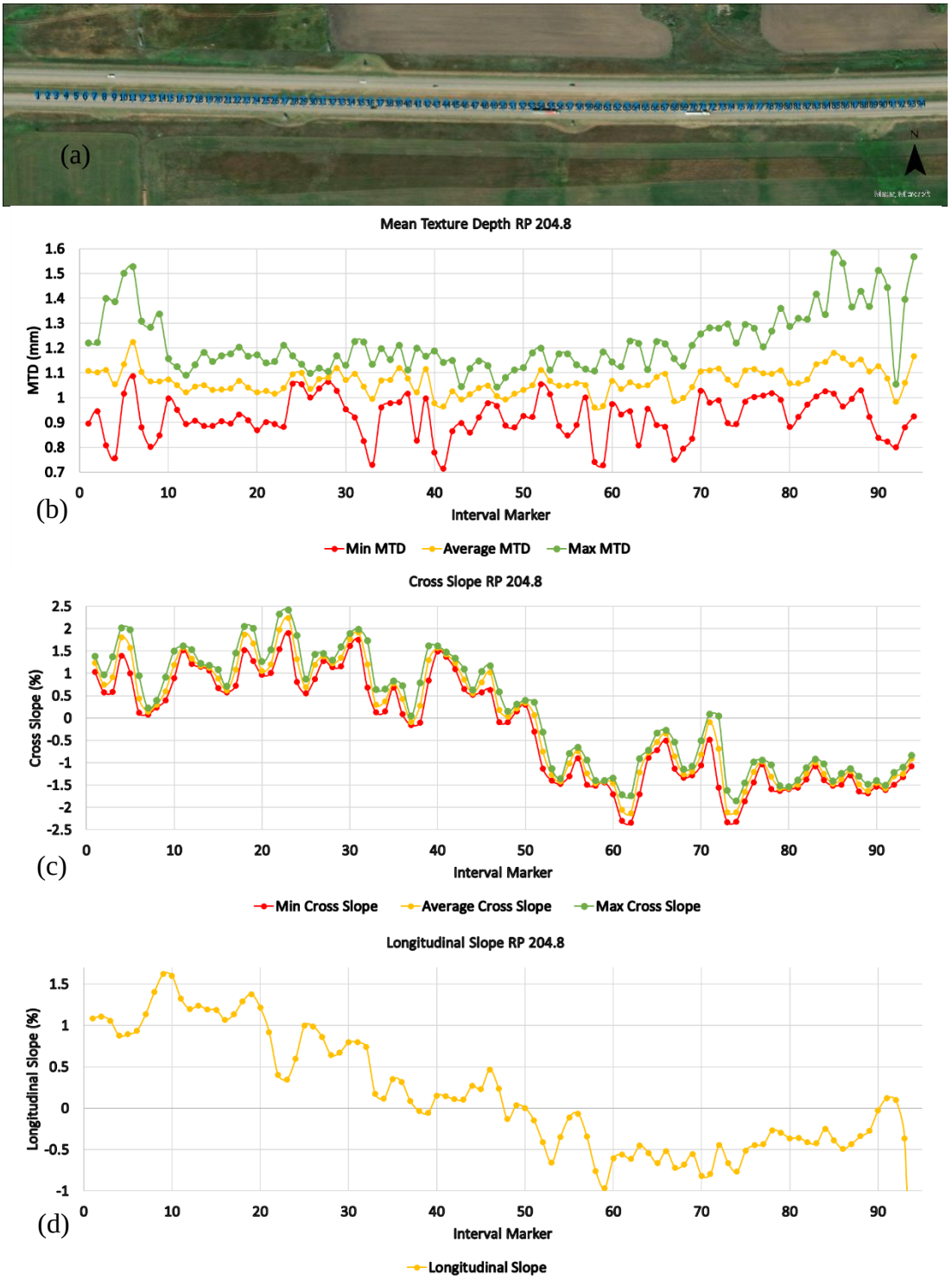

Figure 27: Scan locations (a), MTD (b), cross slope (c), and longitudinal slope for RP 204.8 section.

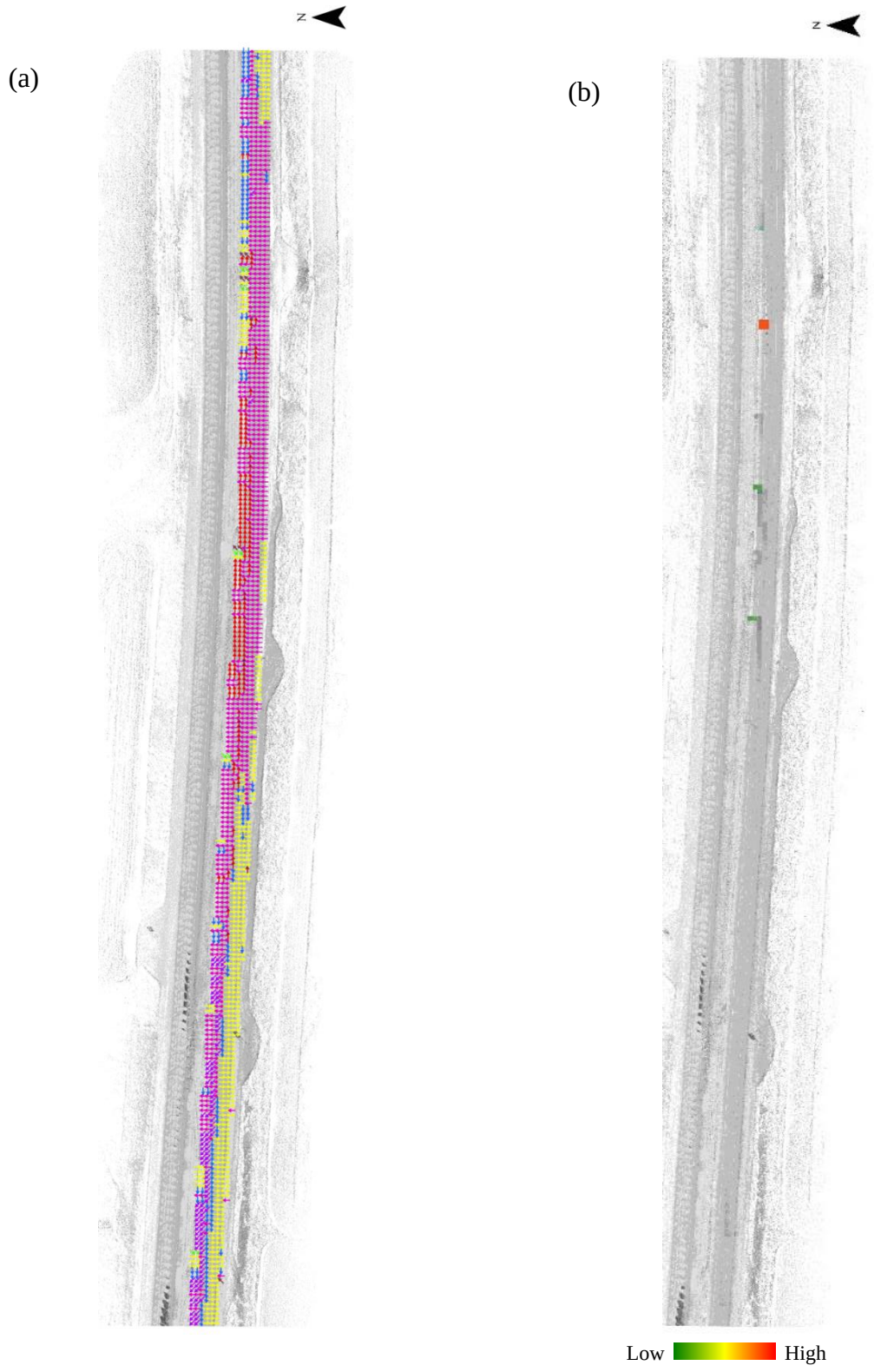

Figure 28: Flow direction (a), and flow accumulation (b) for RP 204.8 section.

At the RP 204.8 location, MTD decreases heading into and out of the horizontal curve, where the minimum texture drops below 0.8 mm. The MTD is adequate for texture, with the average of 1.06 mm and the minimum never falling below 0.5 mm for the section. Notably, both cross slope and longitudinal slope become near zero at the 50th scan interval where a slight amount of flow accumulation can be seen. At the superelevation transition on the east side of the section, and within the horizontal curve at full superelevation, flow direction can be seen traveling across both lanes. This begins to change on the west side of the horizontal curve before the transition. To correct this, a drainage solution can be proposed to correct geometry at that location.

3.1.3 RP 214.7 Results

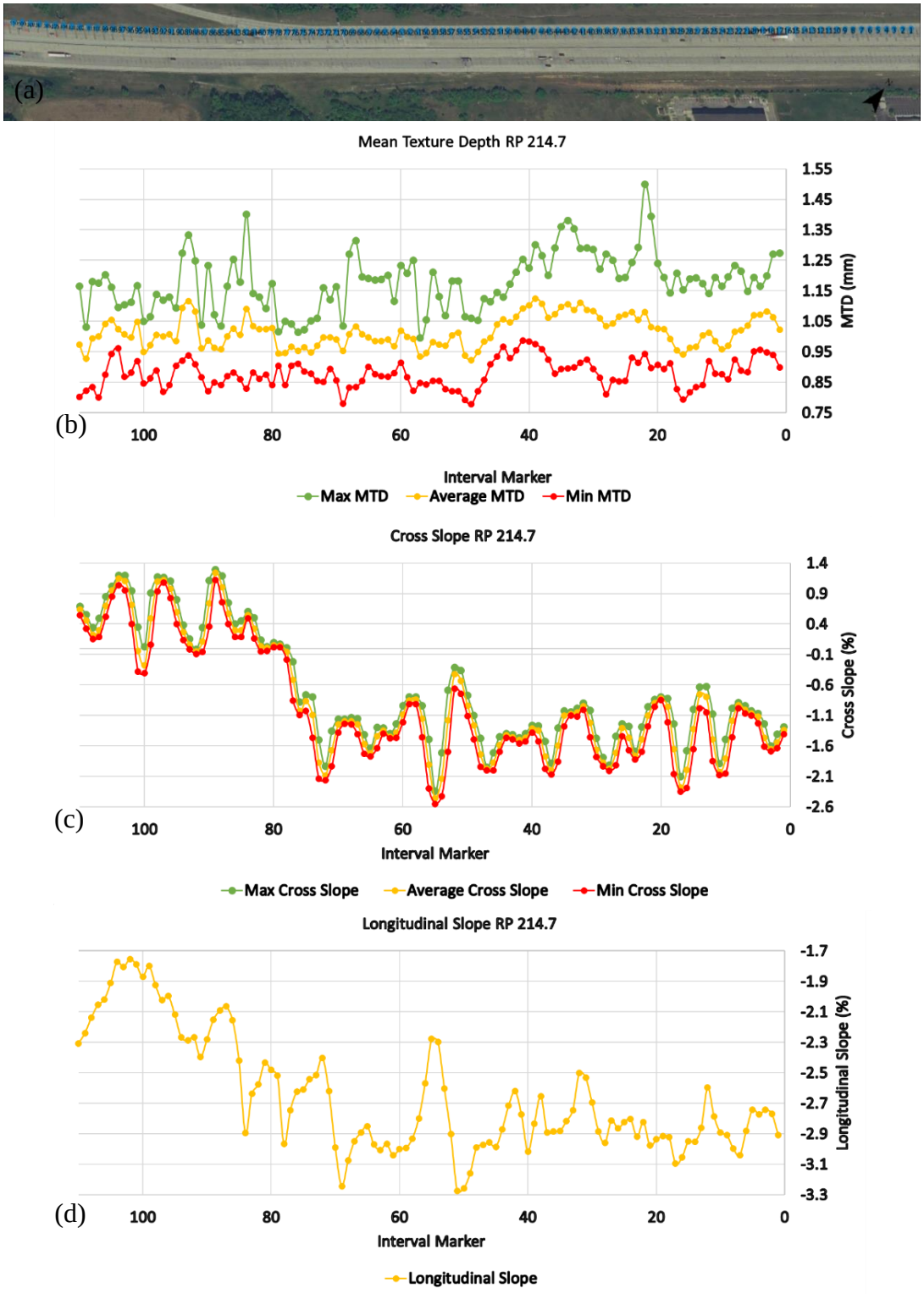

Figure 29: Scan locations (a), MTD (b), cross slope (c), and longitudinal slope (d) for RP 214.7 section.

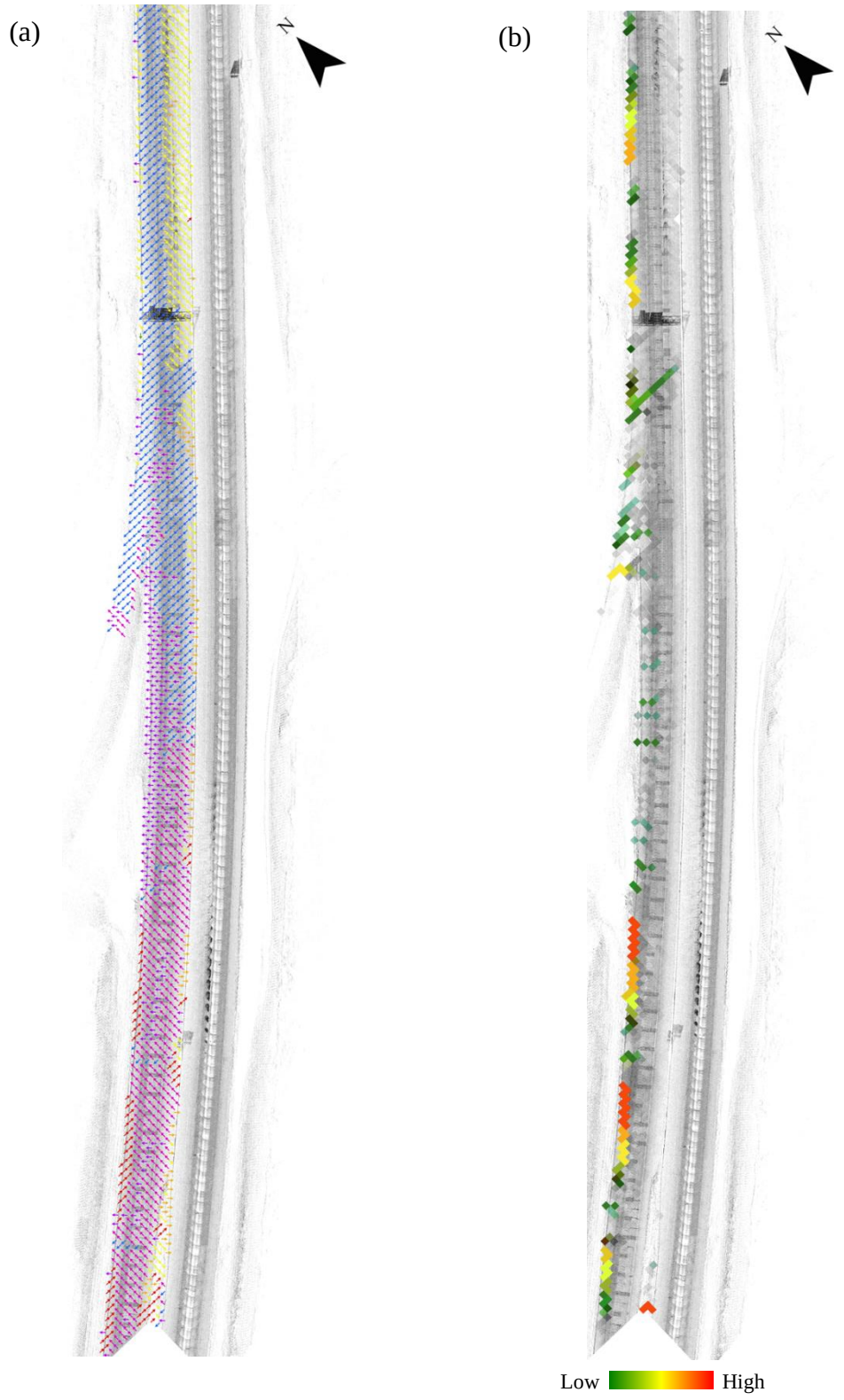

Figure 30: Flow direction (a), and flow accumulation (b) for RP 214.7 section.

At the RP 214.7 location, MTD decreases heading towards the off-ramp. Overall, MTD is adequate for friction with the average MTD of the section being 1.0 mm and the lowest minimum being 0.80 mm. Longitudinal slope is shown here as uphill at a high magnitude in the pathway of travel, indicating that a splash and spray problem may exacerbate the hydroplaning issue reported at this location. The flow direction results also indicated that flow towards the median may be possible and is shown with high water accumulation at the location of the weave. With an adequate MTD, and a flow direction showing flow against traffic, a drainage solution can be proposed to correct geometry at that location.

3.1.4 RP 214.7 Results

Figure 31: Scan locations (a), MTD (b), cross slope (c), and longitudinal slope (d) for RP 217.55 section.

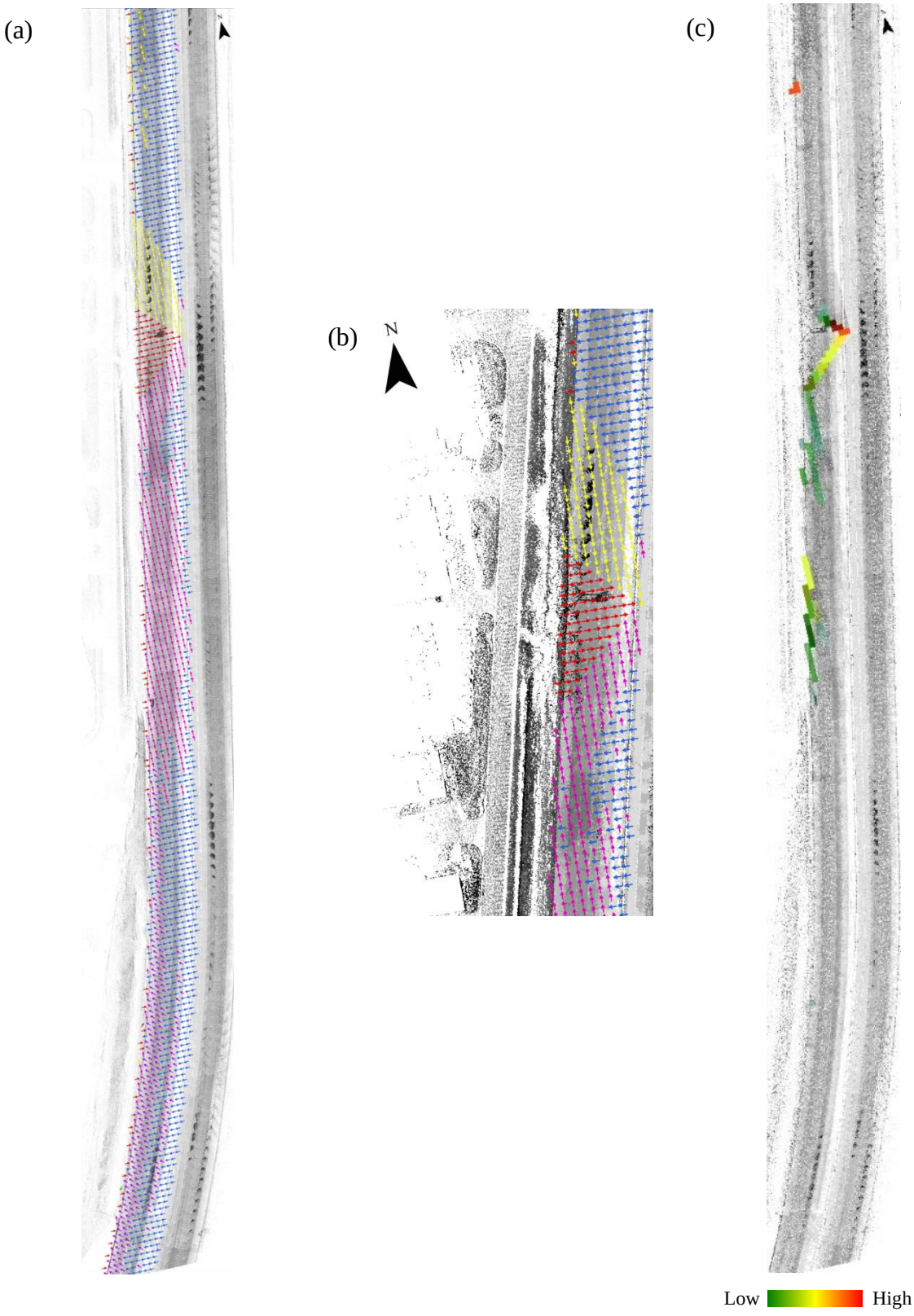

Figure 32: Flow direction (a), enlarged view of flow direction (b), and flow accumulation (c) for RP 217.55 section.

At the RP 217.55 location, the MTD is low over the entire section of roadway, potentially indicating that there is a lack of friction for motor vehicles. The average MTD of the section is 0.75 mm, with a minimum MTD of 0.51 mm. MTD remains the lowest at the area of washout discussed in the site visits section. Flow direction model shows that flow changes directions near this area as well and begins to travel towards the median instead of towards the edge of the roadway. Although the texture at this location is lacking, the drainage of the reversal of flow traveling back on to the roadway should be fixed prior to attending to roadway friction improvements.

3.1.5 RP 295.2 Results

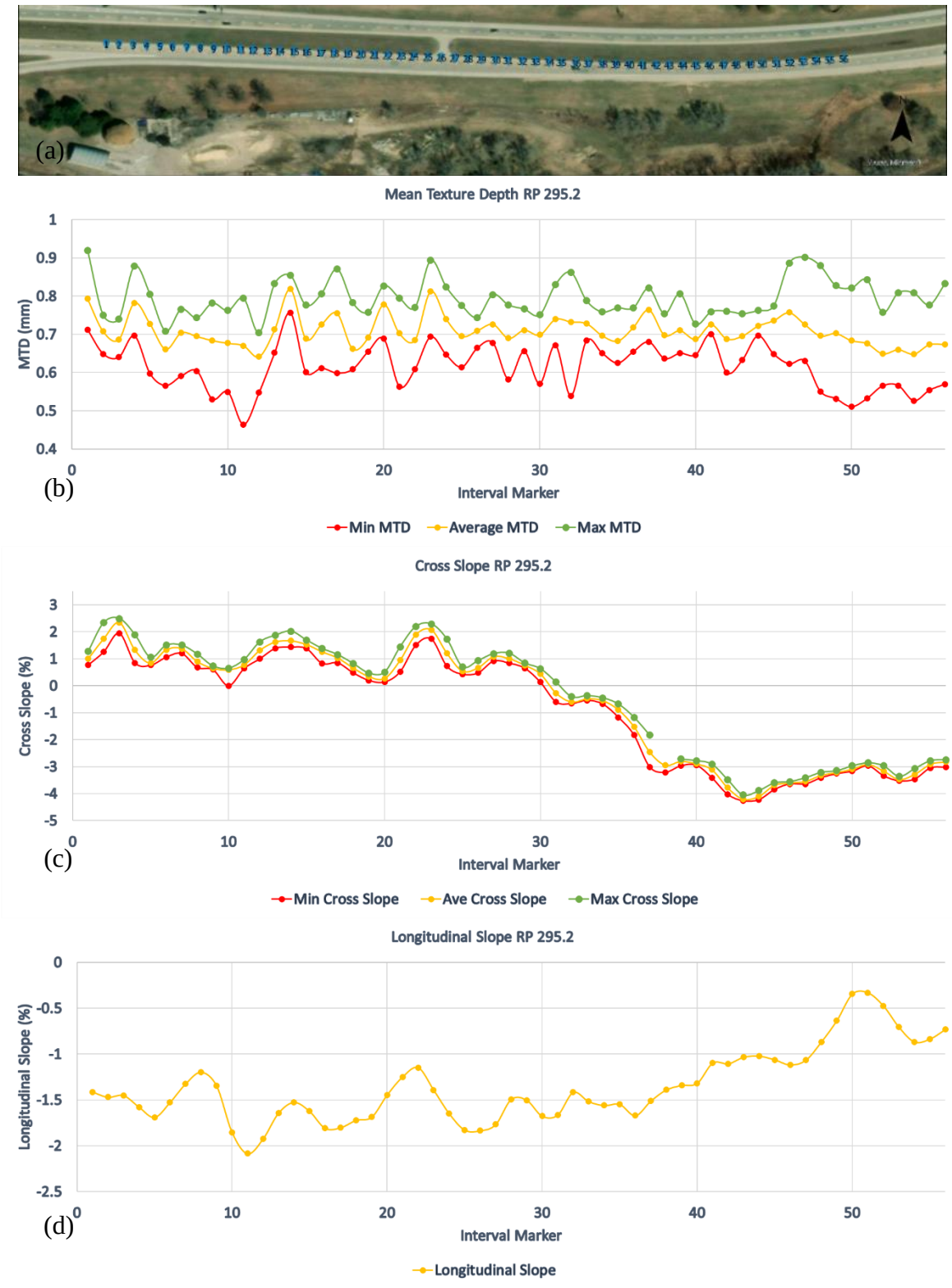

Figure 33: Scan locations (a), MTD (b), cross slope (c), and longitudinal slope (d) for RP 295.2 section.

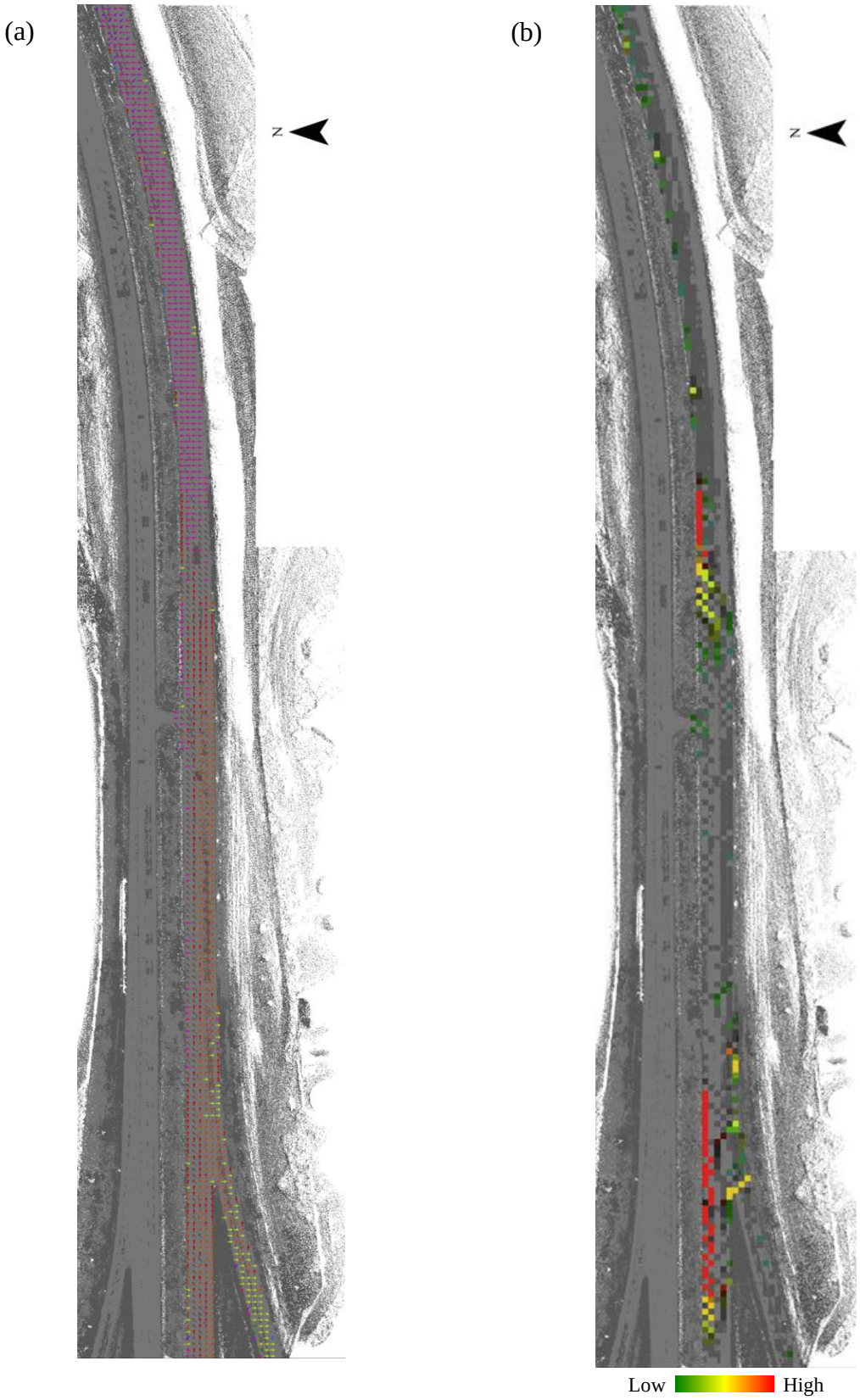

Figure 34: Flow direction (a) and flow accumulation (b) for RP 295.2 section.

At the RP 295.2 location, MTD remains low along the section, which can indicate a lack of texture. The average MTD of the section is 0.71 mm and only rises above 0.8 mm twice in the area. The lowest MTD falls to 0.46 mm, but this is the only time in the section where MTD falls below 0.5 mm. The flow accumulation results for this section are high near the transition area, where the flow direction results indicate flow across the roadway at the end of the merging on-ramp. A texture improvement at this location can be recommended to improve low MTD.

3.1.6 RP 330.1 Results

Figure 35: Scan locations (a), MTD (b), cross slope (c), and longitudinal slope (d) for RP 330.1 section.

Figure 36: Flow direction (a) and flow accumulation (b) for RP 330.1 section.

Out of all the study sites, the RP 330.1 location has the highest MTD where the average MTD is 1.80 mm, and the minimum never falls below 0.5 mm. Even so, the MTD falls near the bridge and creek, as well as near the transition area heading east. The flow accumulation for this section is quite high in many areas. However, digital banding created from the digital terrain scans create uniform flow direction and flow accumulation that can be seen in the east side of the section. Flow direction indicates that changes in direction shift occur at the bottom of the sag curve.

3.1.7 RP 357.7 Results

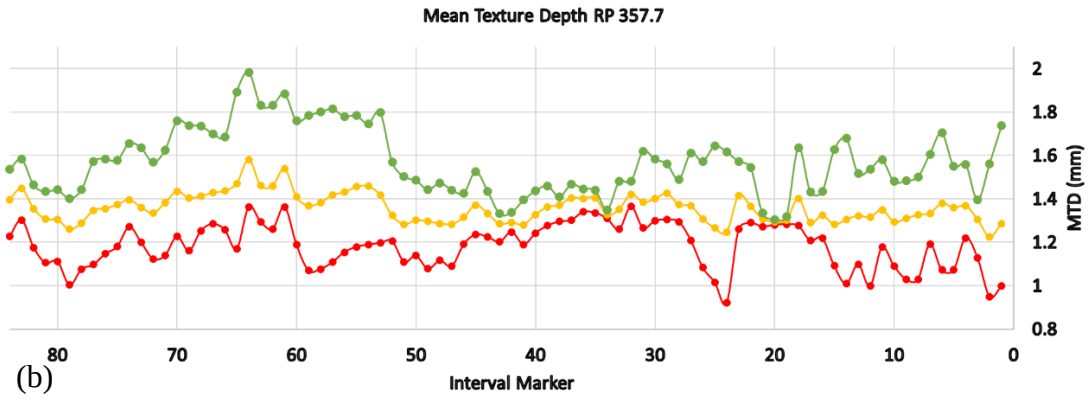

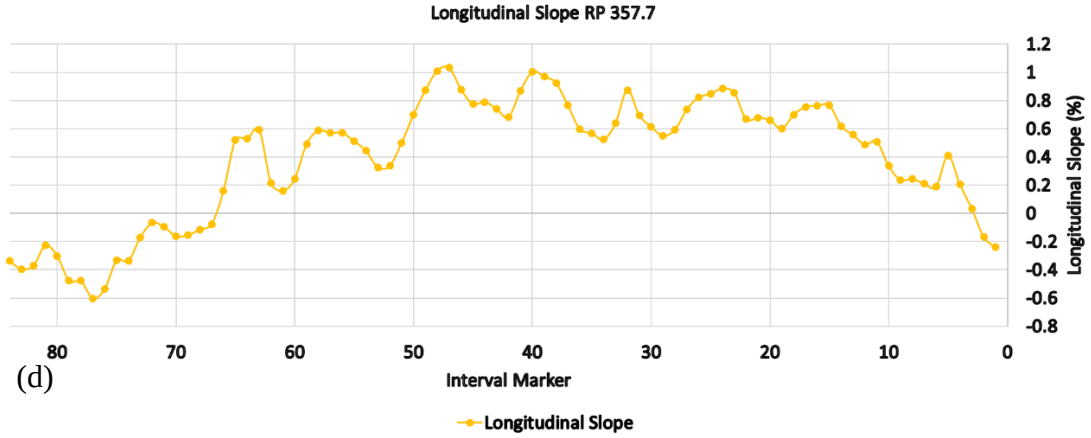

Figure 37: Scan locations (a), MTD (b), cross slope (c), and longitudinal slope (d) for RP 357.7 section.

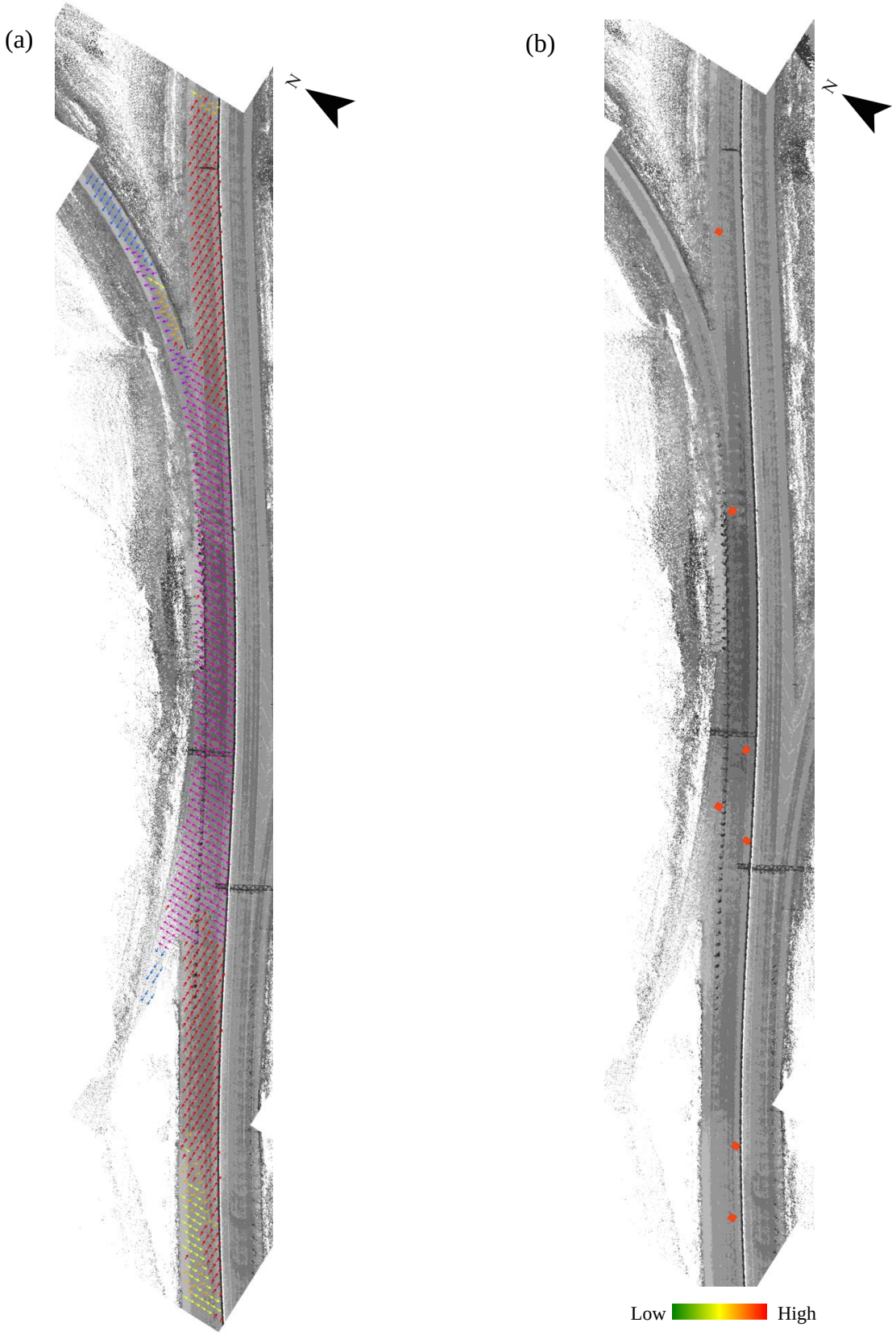

Figure 38: Flow direction (a) and flow accumulation (b) for RP 357.7 section.

For the RP 357.7 location, MTD remains suitable over the section, but dips slightly near the weave terminal. The average MTD over section is 1.36, with MTD never falling below 0.5 mm. Longitudinal slope and cross slope also near zero just after the off-ramp, which can indicate slow drainage. Although the flow accumulation results do not provide much insight into where water might drain to in this roadway, the flow direction results show a reverse of flow that is nearly against traffic, and into the median.

3.1.8 Overall Hydroplaning Potential and Mitigation

A summary of the analysis at each KDOT location is shown in Table 9. Suggestions for each location were based off observations on texture, slope, and flow accumulation and direction made in the previous sections for each location.

Table 9: Study location results.

Location	Average MTD (mm)	Minimum MTD (mm)	Observations	Suggestions Solutions for Investigation
RP 79.2	1.10	0.60	High accumulation at turning lane	Drainage and geometry improvement
RP 204.8	1.06	0.71	Low slope	Drainage and geometry improvement
RP 214.7	1.01	0.80	Drainage flow against traffic	Drainage and geometry improvement
RP 217.55	0.75	0.51	Drainage flow against traffic	Drainage and geometry improvement
RP 295.2	0.71	0.46	High accumulation at super transition and low texture	Texture improvement
RP 330.1	1.85	0.91	High accumulation	Drainage and geometry improvement
RP 357.7	1.35	0.92	Drainage flow against traffic and low slope	Drainage and geometry improvement

Solutions that can be investigated for each of the locations can be found in Table 9. A solution based on improving drainage and/or low-cost geometry remedies such as milling, grinding, and overlays should be considered prior to considering a more expensive geometric redesign.

3.2 Geometric Redesign to Mitigate Hydroplaning

The results summarized in Table 9 indicated that all but the RP 295.2 location of the KDOT study locations suffer from poor drainage and should consider solutions that adjust roadway geometry to improve drainage and reduce the potential of hydroplaning. Due to many suggested

solutions for KDOT locations involving a drainage and geometry redesign, a proof-of-concept highway redesign example was performed in ORD at the RP 295.2 site.

3.2.1 Identifying Poor Drainage Using Flow Paths in ORD

Although literature has pointed to flow path reduction length as a means to mitigate flow at superelevated transitions (Anderson et al. 1998; Brown et al. 2009; Flintsch et al. 2021), descriptions of how to implement this using modern design tools of areas of complicated elements (i.e., ramps, weaves, and intersections) is limited. Therefore, a general method for tracing flow paths using slope in ORD was developed in order to evaluate the effectiveness of the redesign.

The "Aquaplaning" command in ORD was used to identify problematic flow paths in the design. Although a similar method can be performed by drawing perpendicular flow lines between elevation contours, or by using flow arrows, the Aquaplaning tool allows the user to observe areas where concerning flow paths exist more easily in a highway design. This tool also contains integration with the WFT equation by Gallaway et al. (1971) and another WFT equation by the Road Research Laboratory in the United Kingdom that uses similar inputs. These empirical equations are available for use, but as discussed previously, have poor effectiveness at areas of complicated geometry, so they were not used for this example.

The Aquaplaning command was used with the following settings: a flow interval of 10 ft, rainfall intensity 0f 2.00 in/hr, a shallow ridge slope of 0.00 percent, a maximum film depth of 0.007 ft (2.1 mm), a maximum slope of 20.0 percent, a texture depth of 0.002 ft (0.7 mm), the Gallaway formula selected, and "use equal area slope" unselected. Since this is a 2-lane roadway, flow would drain off to each edge from the crown if designed with drainage in mind. The trace slope tool displays this as a result in two separate directional lines that travel away from the crown of the road. The roadway profile with flowlines plotted every 10 feet at the crown of the road can

be seen in the figure below where the roadway lanes are shown in black, the crown is shown in red, and the flow lines are shown in green with blue flow lines indicating areas with flow above the maximum flow depth (according to the Gallaway formula). An orange line was drawn to designate the beginning of the superelevated transition, a red line for when the right lane experiences a slope of zero, a yellow line for when 75 percent of the superelevation is reached in the runoff length, and a purple line signifies full superelevation. The flow slope lines were isolated for clarity.

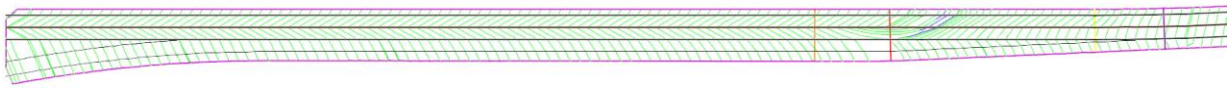

Figure 39: Flow slope paths of original RP 295.4 design.

The slope direction from the crown can be seen as a pathway to the roadway edges and across the acceleration lane. Flow across the acceleration lane is less of a concern, as vehicles in this area would travel at a lower speed than on the mainline, resulting in lower likelihood of hydroplaning.

Near the superelevation transition, the slope lines begin to group together instead of forming parallel bands like before. This would indicate that flow would accumulate in the areas where slope flow lines overlap with each other if originating from different locations. Since the flow lines are also in the direction of traffic, vehicles would be able to push water down the roadway in a splash and spray scenario to potentially exacerbate the drainage issue. A closer view of the transition area can be seen in the figure below.

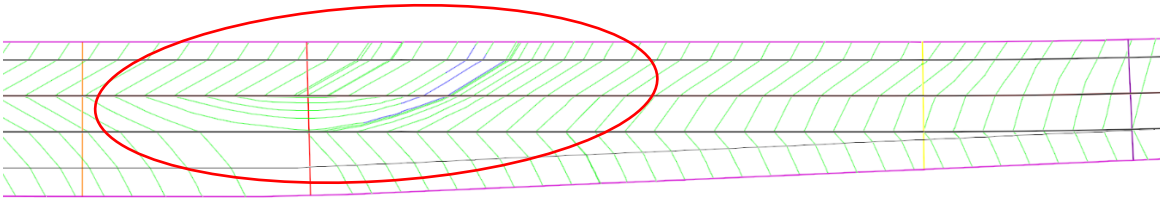

Figure 40: Flow slope path of transition area of original RP 295.4 design.

This change in flow slope path direction can be visuality compared to the sections of the roadway before the superelevation transition as seen below.

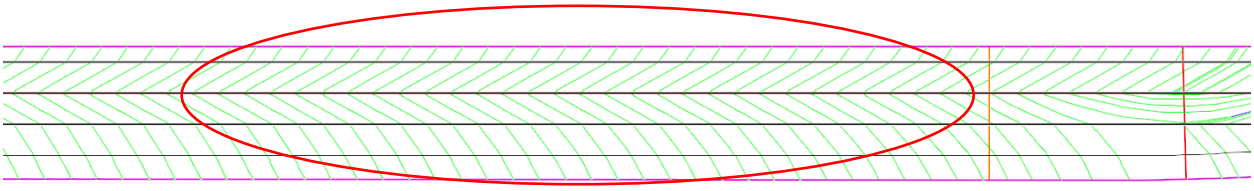

Figure 41: Flow slope path of tangent section of RP 295.4 location.

After an area that exhibits indications of limited drainage, steps can be taken to adjust the design. Although it is understood that adjusting a current, built design would only take place as a last recourse, the following design changes proposed to this location can be considered for future design of superelevated transitions.

Considering a shorter superelevated transition length at this location could reduce the length of roadway where the cross slope is near zero. This would allow for water to drain from the transition area faster as cross slopes surrounding the transition would be increased and would result in shorter flow slope lines. An evaluation of the transition length was considered as the minimum runoff length and minimum runoff length were calculated using the Green Book.

A design speed (V_D) of 70 mph, an e_{max} of 8.0 percent, a design superelevation (e_d) of 6.5 percent, and a maximum relative gradient (Δ) for a design speed over 50 mph of 0.50 was used. The radius of the horizontal curve was kept identical to the design curve. Considering the minimum

runoff length using the equation below, a minimum runoff length (L_r) of 156 feet was found. The lane width (w) is 12 feet, the number of lanes rotated (n_l) is 1, and the lane adjustment factor (b_w) is 1.

$$L_r = \frac{(wn_l)e_d}{\Delta}(b_w) \quad [12]$$

The minimum runout length (L_t) was found to be 37.44 feet using the equation below where the normal cross slope rate (e_{NC}) is 1.56 percent, and L_r is 156 feet.

$$L_t = \frac{e_{NC}}{e_d}L_r \quad [13]$$

A method of attaining superelevation as shown in the figure below that matched the original design plans was used with 75 percent of the runoff length occurring before the PC.

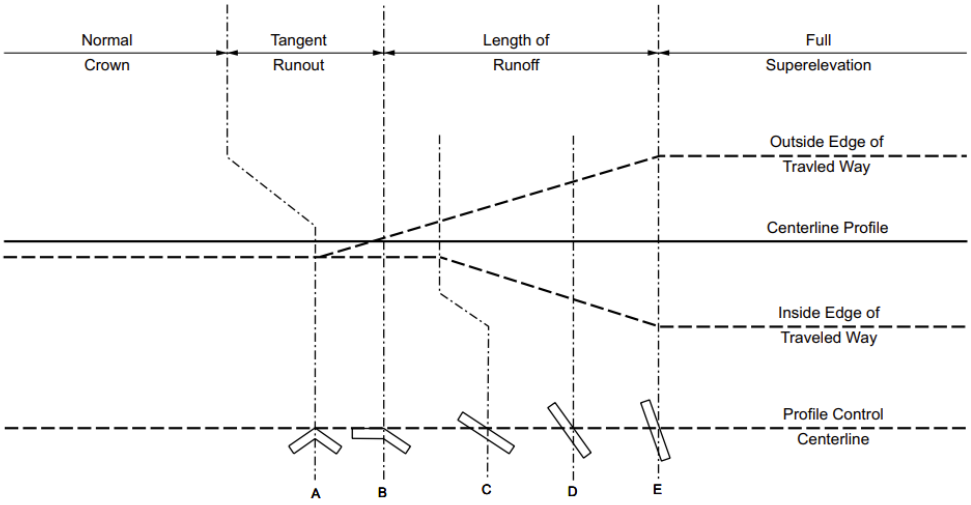

Figure 42: Method of attaining superelevation for transition redesign (AASHTO, 2018).

Creating a superelevation transition of the minimum length could be jarring and visually unattractive for drivers. The minimum transition lengths for both of the runout and runoff lengths were increased by one quarter (shown as Transition 1) and by one third (shown as Transition 2) to

create smoother transitions. Although the runout length used in Kansas is typically 75 ft, shorter lengths were used to demonstrate flow path length reduction in this example. Statistics about the calculated transitions can be found in the table below.

Table 10: Comparison of transition designs created for RP 295.4 location in ORD.

Transition	**Rounded Runout Length (ft)**	**Rounded Runoff Length (ft)**	**Amount Shortened Compared to Original Design (%)**
Minimum	38	156	- 44.6
1	47	195	- 30.9
2	50	208	- 26.3
Original Design	75	275	N/A

Heading into the horizontal curve, the longitudinal slope of the roadway transitions from -2.66 to -0.05 percent. Referencing the vertical alignment of the design seen in the figure below, the superelevated transition occurs at the beginning of the sag vertical curve. The start and end of the transition is marked with vertical, pink lines. The longitudinal slope at the beginning of the transition is -2.66 percent, while the longitudinal slope at the end of the transition is -1.06 percent.

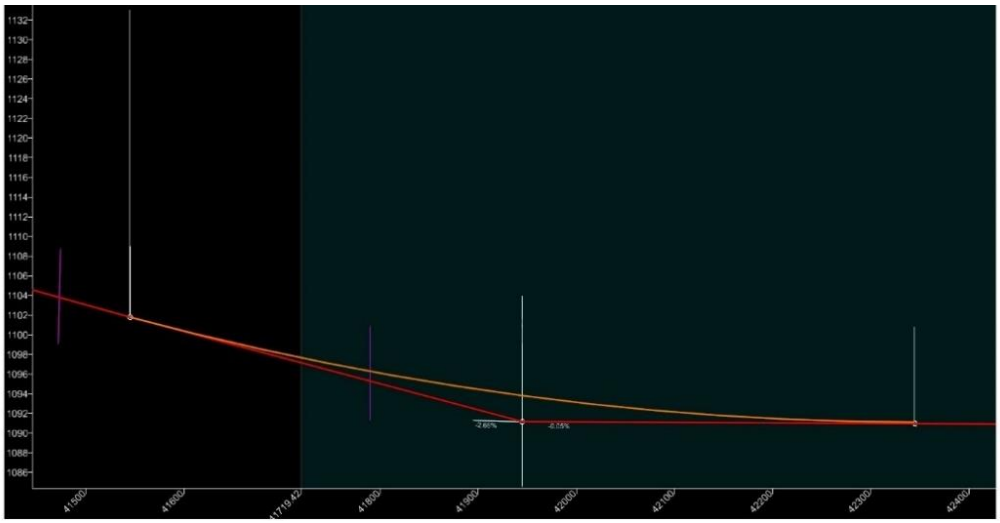

Figure 43: Vertical alignment for RP 295.4 location.

The bottom of the vertical sag curve created by this transition occurs near the middle of the horizontal curve. Grade near the transition to the sag curve can be deemed suitable for drainage by using Section 3.3.8.9 in the Green Book. The first consideration for this section is to ensure that the minimum profile grade of 0.5 percent is used. Within the transition area, the profile grade is above 0.5 percent. The second technique is to ensure that a minimum of 0.2 percent edge-of-pavement grade for uncurbed sections is used. The following equations should be used as seen below for verification. Here, Δ^* is the effective maximum relative gradient (%), w is the width of one lane (ft), n_l is the number of lanes rotated, e_d is the design superelevation (%), L_r is the superelevation runoff length (ft), and G is the profile grade (%).

$$\Delta^* = \frac{(wn_l)e_d}{L_r} \quad [14]$$

$$G \leq -\Delta^* - 0.2 \quad [15]$$

$$G \geq -\Delta^* + 0.2$$

$$G \leq \Delta^* - 0.2$$

$$G \geq \Delta^* + 0.2$$

Using values form the original design, the effective maximum relative gradient was found to be 0.28 percent, and the bounds of the control grades was found to be -0.48 percent and +0.48 percent. The grade within the transition area remains outside the range of these values resulting in the transition to meet both of the criteria for proper drainage at the beginning to the horizontal curve.

One solution considered was to adjust the acceleration lane to lessen splash and spray from vehicles merging to the mainline. Beginning on Section 10.9.6.4.7 in the Green Book titled "Speed-Changes Lanes" describes entrance terminal lane design for on-ramps and off-ramps. Noted in the Green Book, there are the two types of entrance terminals: the taper type and the parallel type entrances are shown below from Figure 10-72A in the Green Book.

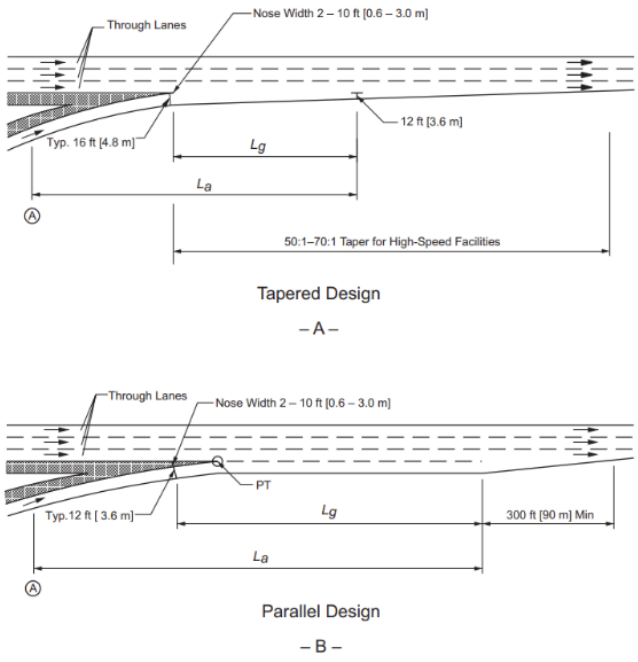

Figure 44: Entrance terminal examples from the Green Book (AASHTO 2018).

Adjusting the acceleration lane to ensure that it does not merge with the through lanes at the superelevated transition would allow for better drainage and minimize merging vehicles from spraying water onto the mainline during a rain event. However, creating a shorter acceleration lane would not be possible in this area. A tapered design would not allow for enough space before the horizontal curve. Shortening the ramp would not be ideal, as its current length is suitable for the design speeds as per Table 10-4 in the Green Book. A portion of Table 10-4 can be seen below.

Table 11: Minimum acceleration lane lengths from Green Book (2018) Table 10-4.

Acceleration Lane Length, L_a (ft) for Design Speed of Controlling Feature on Ramp, V' (mph)										
Highway		Stop Condition	15	20	25	30	35	40	45	50
Design Speed, V (mph)	Merge Speed, V_a (mph)	Average Running Speed (i.e., Initial Speed) at Controlling Feature on Ramp, V'_a (mph)								
		0	14	18	22	26	30	36	40	44
30	23	180	140	-	-	-	-	-	-	-
35	27	280	220	160	-	-	-	-	-	-
40	31	360	300	270	210	120	-	-	-	-
45	35	560	490	4.4	380	280	160	-	-	-
50	39	720	660	610	550	450	350	130	-	-
55	43	960	900	810	780	670	550	320	150	-
60	47	1200	1140	1100	1020	910	800	550	420	180
65	50	1410	1350	1310	1220	1120	1000	770	600	370
70	53	1620	1560	1520	1420	1350	1230	1000	820	580
75	55	1790	1730	1630	1580	1510	1420	1160	1040	780
80	57	2000	1900	1800	1750	1680	1600	1340	1240	980

An adjustment that can be made is in the form of an entrance ramp on the horizontal curve to avoid the acceleration lane merging with the mainline during the superelevation transition. An example of this can be seen in Figure 10-75 in the Green Book.

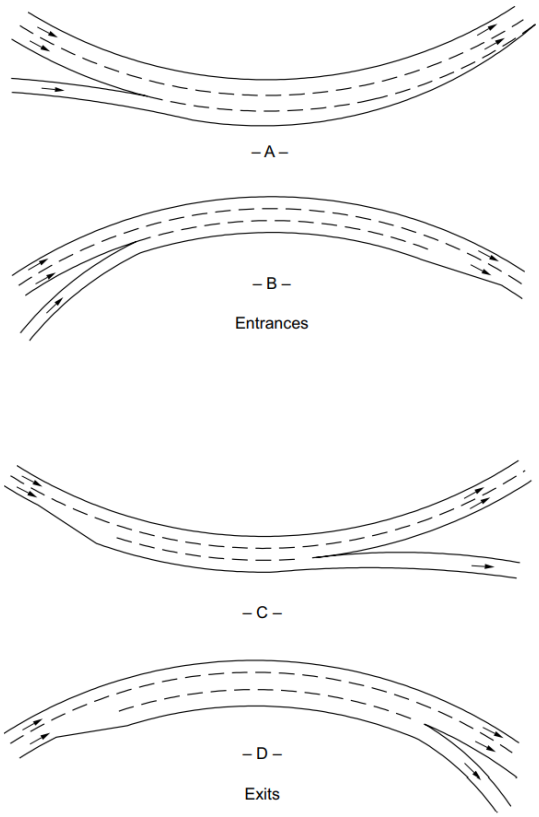

Figure 45:Entrance types that occur within horizontal curves from Green Book (AASHTO 2018).

In the case of this location, an entrance ramp like "A" in the figure above can be used at this location. Found in the Green Book Section 10.9.6.6.3 "Free-Flow Terminals on Curves," the guide for the design of these types of entrances and exits is found. Following the method for developing the taper of the speed change lane was used to complete the redesign example for the RP 295.4. This can be seen in the results section.

3.2.2 Design Check for Potential Hydroplaning

Transition length, longitudinal grade, and roadway reconfiguration was performed using slope path flow reduction as a means of evaluating each design. When a check for adequate longitudinal slope was performed, the current design was found to be acceptable, and no redesign was conducted for this subject. Results for transition length adjustment and acceleration lane reconfiguration are shown below.

It was found that reducing the transition length did not have a linear decrease in flow path. The redesigned transition of longer length was seen yielding a slightly shorter flow path. With this in mind, it is recommended that KDOT should evaluate multiple variations of a design when using minimization of slope flow paths.

Table 12: Decrease in slope flow path length seen transition redesign.

Transition	**Length of Longest Flow Path on Transition (ft)**	**Flow Path Length Reduction Compared to Original Design (%)**	**Amount Transition Shortened Compared to Original Design (%)**
1	99.0	- 21.3	- 30.9
2	96.0	- 23.7	- 26.3
Original Design	125.8	N/A	N/A

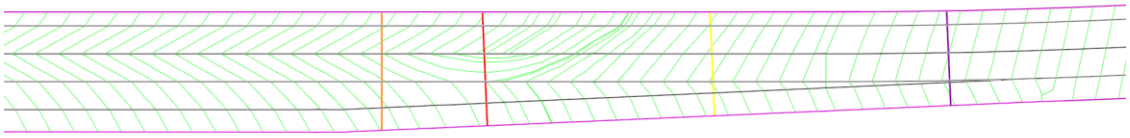

Figure 46: Transition design 1 for RP 295.4 location.

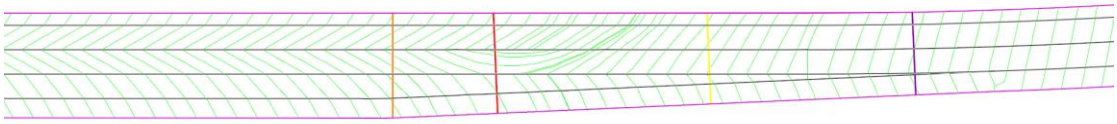

Figure 47: Transition design 2 for RP 295.4 location.

Another option explored during research was whether to adjust the configuration of the on-ramp. An example roadway mesh of this can be seen below in ORD. The acceleration lane takes place completely within the horizontal curve. The acceleration lane ends at three-quarters of the length of the horizontal curve, has a taper of 50:1, and follows the same profile as the on-ramp of the original design.

Figure 48: Acceleration lane reconfiguration at RP 295.4 location

This configuration does not correct the flow lines found in the original design, but moving the acceleration lane to the horizontal curve to avoid the superelevation transition may improve splash and spray drainage in the area. With the addition of the shoulder adding to the transitioning compared to the acceleration lane that sloped to the outward edge during the transition, a longer flow path was created. Slope paths representing drainage flow can be seen in the figures below from ORD. The slope paths were drawn every 10 feet using the Aquaplaning tool.

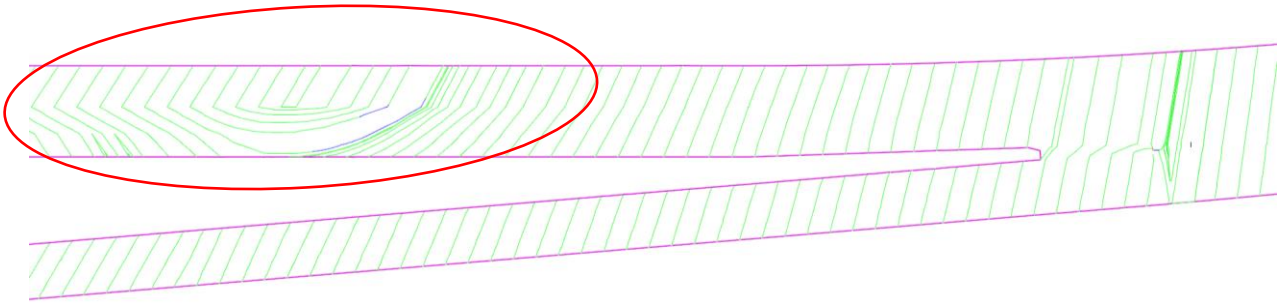

Figure 49: Slope flow path length for acceleration lane reconfiguration at RP 295.4 location.

Due to the lengthening of the flow path above that of the original design, this configuration could be outweighed by other redesign options.

3.3 Broader Implications of Hydroplaning in Kansas

Analysis of hydroplaning mitigation was conducted at seven sites selected by KDOT, however, this analysis does not consider whether these locations are representatives over the broader highway system in Kansas. In order to consider the broader implications across Kansas' highway system, this research examined 200 thousand crashes from 2011-2021. In the first section (Section 3.3.1) the results of clustering crashes across the state of Kansas are presented. This is then followed by Section 3.3.2 which discusses how the crash data when combined with precipitation data can provide insights into potential areas of hydroplaning across the state.

3.3.1 Clustering Crashes

The number of resulting clusters was compared when three different cluster threshold distances (500 m, 1000 m, and 1500 m) were used. A 500-meter distance threshold identified a total of 18,632 total clusters, 1000-meter distance threshold identified 10,268 clusters, and a 1500-meter distance threshold identified 7,081 clusters. The locations of the clusters depending on threshold distance can be seen in the figures below. The figures show that more crashes were placed into a single cluster as the threshold distance was increased. Based on the distances of the KDOT study locations, a distance of 1000 meter was chosen as the threshold distance. This distance reasonably encompassed the section lengths of study locations while not including sections not involved with the study.

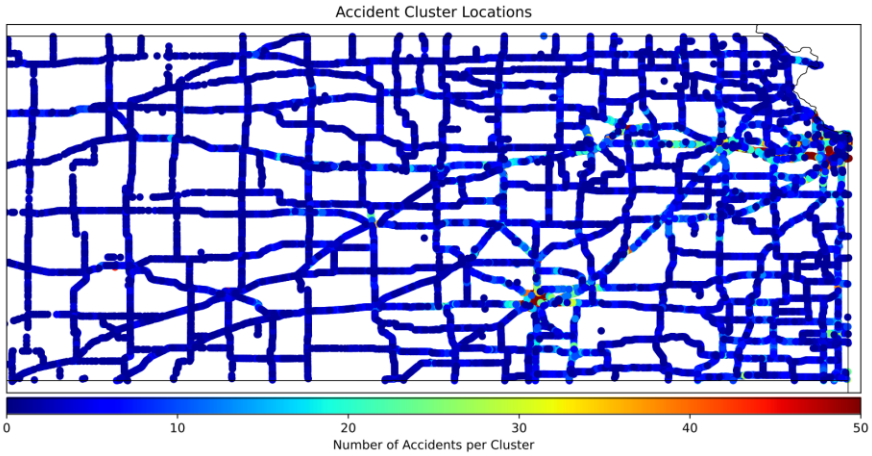

Figure 50: Crash cluster locations using distance threshold of 500 m.

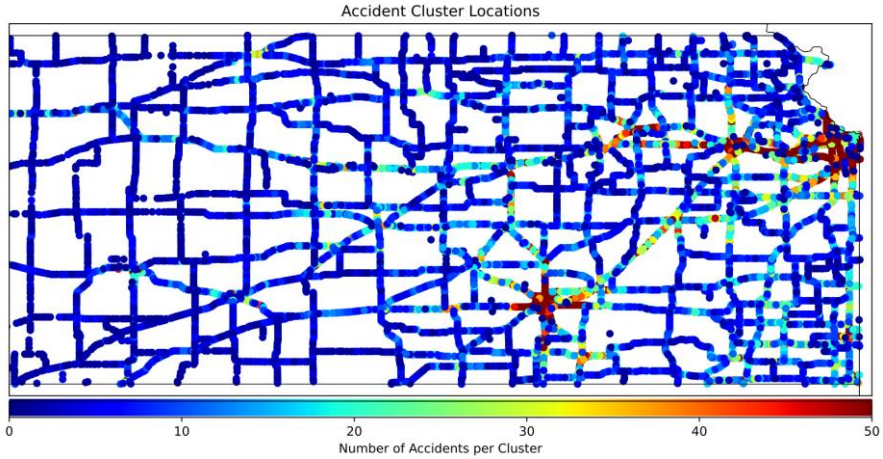

Figure 51: Crash cluster locations using distance threshold of 1000 m.

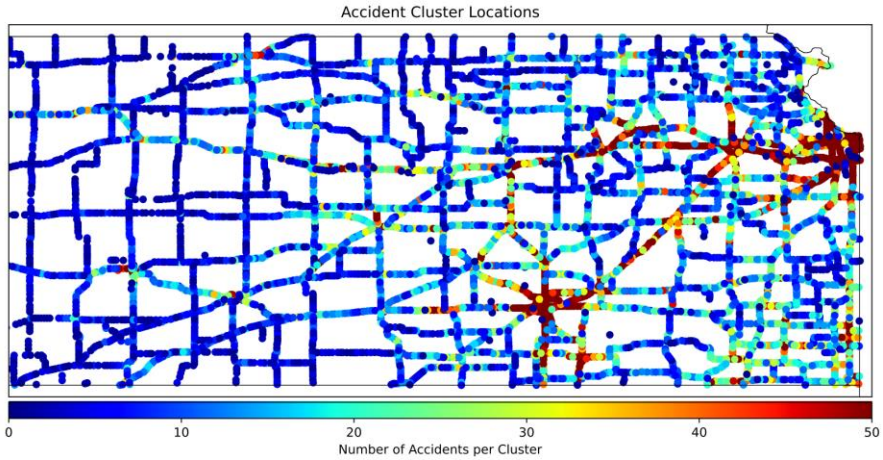

Figure 52: Crash cluster locations using distance threshold of 1500 m.

3.3.2 Potential Hydroplaning Hotspots

A total of 10268 clusters were identified using the distance-threshold method and were combined with hourly precipitation to identify hydroplaning "hotspots" where a high number of wet-weather crashes occurred. In order to determine hydroplaning hotspots, the percent of crashes that occurred during wet conditions was calculated. A crash is considered to occur during wet-weather if there is a rain event within +/- 2 hours within the time of the reported crash base on the NLDAS data. A two-hour buffer is used to account for uncertainty in crash time, timing of the hourly precipitation and difference between daylight saving time. Figure 53 shows the distribution of percent crashes that occurred during wet conditions. As seen in the Figure 53, over half of the clusters experienced less that 30 percent of their crashes during a time with precipitation.

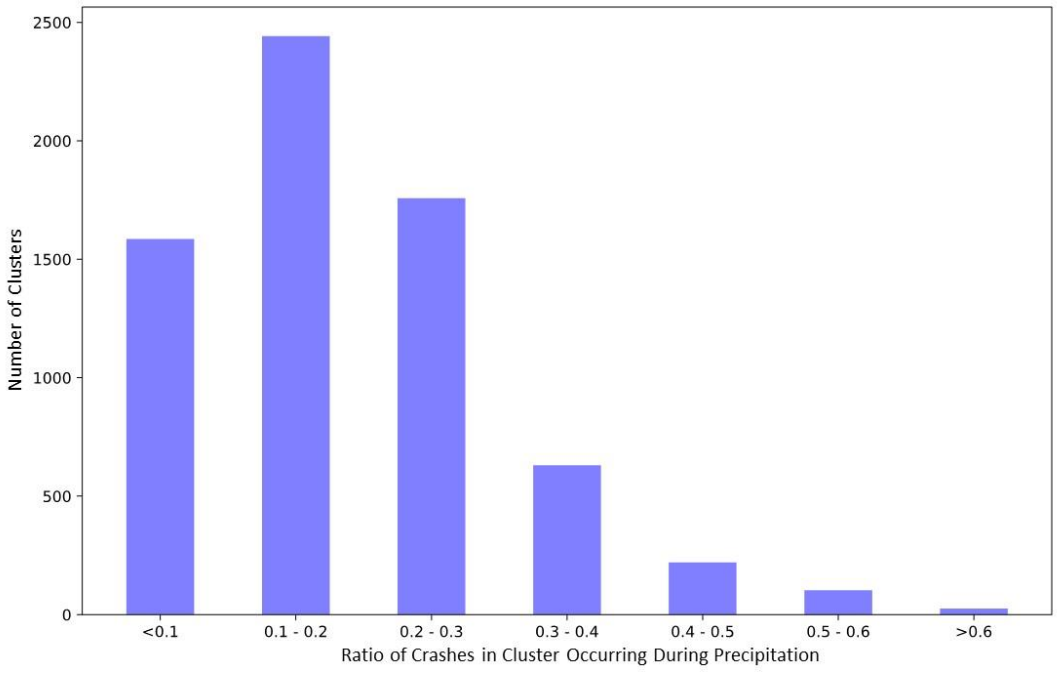

Figure 53: Number of crash clusters with percent of crashes occurring during precipitation.

Hydroplaning hotspots are identified as clusters with at least six crashes and having over 60 percent of the crashes occurring during wet weather. Based on this threshold, 26 crash clusters

were identified as hydroplaning hotspots. Table 13 gives a summary of the potential hotspots and Figure 54 provides a map of the hotspots.

Table 13: Hydroplaning hotspots based on crash and precipitation data.

Cluster ID Number	**Latitude**	**Longitude**	**Total Crashes in Cluster**	**Ratio of Crashes Occurring During Rain Event**
1	39.329422	-101.86331	6	0.67
2	39.56231	-96.7543	7	0.71
3	38.034912	-100.88345	6	0.67
4	38.06139	-94.70999	10	0.6
5	39.57698	-101.054436	7	0.71
6	39.06908	-98.15126	6	0.83
7	37.76021	-97.00196	86	0.62
8	38.44074	-95.68082	11	0.64
9	38.152863	-96.49227	24	0.62
10	37.157745	-97.339455	28	0.61
11	38.2322	-96.40461	43	0.65
12	38.84987	-97.647125	44	0.61
13	38.18108	-96.46171	55	0.76
14	37.725437	-99.32313	6	0.83
15	39.329487	-101.65421	12	0.67
16	38.650455	-95.23229	11	0.64
17	37.178707	-94.86881	7	0.71
18	37.040928	-97.49226	10	0.6
19	38.163666	-96.48202	28	0.68
20	37.66494	-96.71248	8	0.88
21	38.081585	-95.203384	6	0.67
22	38.208084	-98.74819	8	0.62
23	39.77102	-98.959656	6	0.67
24	38.84936	-98.169075	15	0.6
25	39.020023	-99.916855	6	0.67
26	38.528603	-96.13807	6	0.67

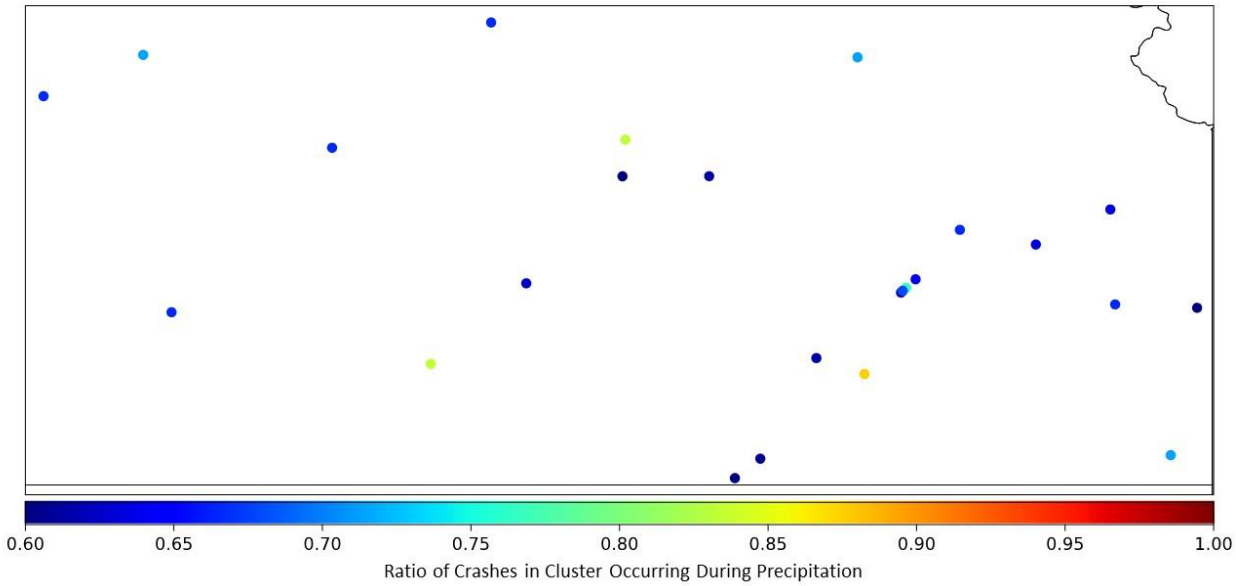

Figure 54: Crash clusters with high precipitation.

The KDOT selected study locations can be compared to the hydroplaning hotspots from the crash data. This is done by identifying the nearest crash clusters to the coordinates of the KDOT study locations. Like the clusters of the entire state, these clusters do not consider the direction of travel associated with the crash.

Table 14: Clusters closest to KDOT study locations.

Reference Point (RP)	Cluster Latitude	Cluster Longitude	Total Crashes in Cluster	Ratio of Crashes Occurring During Rain Event
79.2	39.067017	-95.72994	363	0.29
204.8	38.84885	-98.484	20	0.35
214.7	38.99972	-96.86044	254	0.30
217.55	38.067623	-95.37895	16	0.38
295.2	38.40518	-96.48997	9	0.22
330.1	38.848427	-94.82388	73	0.42
357.7	38.883774	-94.791336	825	0.28

The clusters near the KDOT selected study locations have far lower crashes that occur during wet-weather when compared to the cluster using crash data across Kansas.

A map plotted with the clusters that experienced increased amounts of wet-weather crashes can be seen in Figure 55.

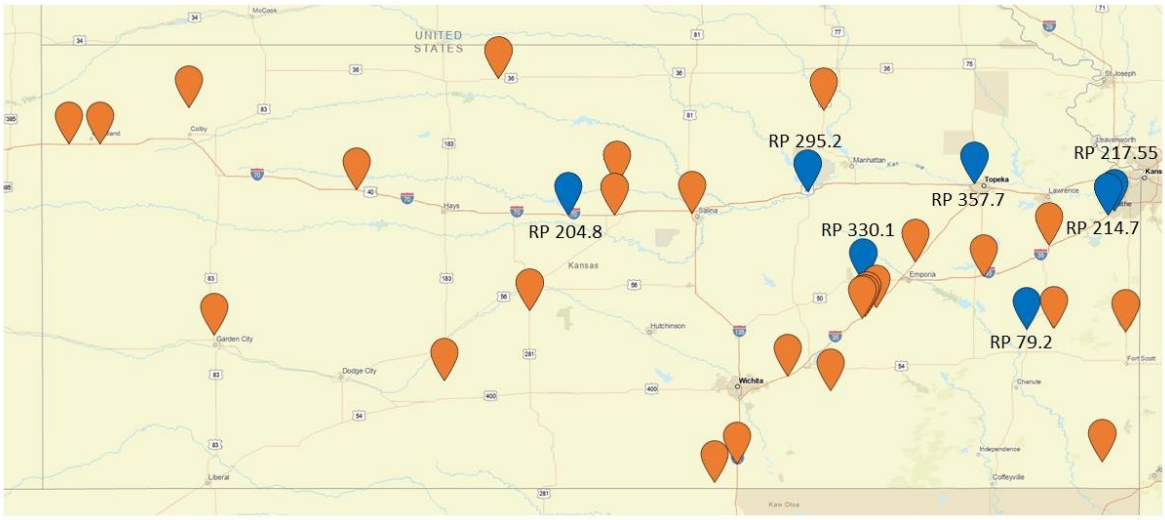

Figure 55: Wet-weather clusters (in orange) and study locations (blue).

The wet-weather clusters with more than 20 crashes were investigated by observation seen in the figures below. All but cluster #10 was near superelevated transition areas. Although the cluster hotspots with the highest number of crashes were located near superelevated transitions, it cannot be assumed that the hydroplaning at superelevated transition is the main cause of high wet-weather accidents. A table and figures of these locations can be seen below.

Table 15: Wet-weather clusters with more than 20 crashes.

Cluster ID Number	**Total Accidents in Cluster**	**Percent of Accidents Occurring During Precipitation Event**
7	86	0.62
9	24	0.62
10	28	0.61
11	43	0.65
12	44	0.61
13	55	0.76
19	28	0.68

Figure 58: Cluster ID number 7 (left) and cluster ID number 9 (right).

Figure 57: Cluster ID number 10 (left), 11 (middle), and 12 (right).

Figure 568: Cluster ID number 13 and cluster ID number 19.

None of the study locations that had a high number of hydroplaning reports were located near the clusters of high wet-weather crashes. There are several reasons why the KDOT locations were not identified from the broader analysis. First, the locations selected by KDOT were based on expert knowledge and familiarity of the locations. That means the study locations are prone to be visited by KDOT engineers. Several of the locations selected by KDOT are nearby to KDOT maintenance centers. So, while the KDOT locations may be regionally problematic, they have the potential to not be as problematic as other areas across the state.

A second reason why the KDOT areas were not identified in the hydroplaning clusters could be that the 1000-meter clustering distance may have been too large. A wet problematic area combined with a non-wet problematic area could have a diluted impact. Likewise, not considering the direction of the crash could also have a similar impact by combining crashes in the same analysis cluster which could lessen the impact of wet-weather-based crashes on the crash cluster statistics. While the locations identified by KDOT are problematic for hydroplaning, there are other locations across the state that are prone to hydroplaning and could present a much higher safety risk.

To explore how traffic volume played a role in the number of crashes in a cluster, the crash rate was calculated for the KDOT locations as well as the high wet-weather crash cluster locations with more than 20 accidents. Crash rates were calculated using the equation below from Federal Highway Administration report number FHWA-SA-11-09 by Golembiewski and Chandler (2011), where R is the roadway departure crash rate for the road segment expressed as crashes per 100 million vehicle-miles of travel, C is the total number of roadway departure crashes in the study period, V is the traffic volumes using Average Annual Daily Traffic (AADT) volumes, N is the number of years in the study period data, and L is the length of the segment in miles. Here, the

2021 AADT volume (V) was used, the study period (N) was 11 years, and the length of the segment (L) was the length of a cluster (1000 m or 0.621 miles).

$$R = \frac{C \times 100{,}000{,}000}{V \times 365 \times N \times L} \quad [12]$$

Crash rates were calculated for KDOT location sites and clusters with more than 60 percent wet-weather crashes that had more than 20 accidents during the study period. Results of this can be seen in the tables below where crash rates are given for each location as well as the accident rate during wet weather. Wet-weather crash rates only considered crashes that were indicated as occurring during wet weather.

Table 16: Crash rates for clusters nearest to KDOT study location during study period.

Reference Point (RP)	**Cluster Latitude**	**Cluster Longitude**	**Total Crashes in Cluster**	**Ratio of Crashes Occurring During Rain Event**	**Annual Average Daily Traffic as of 2021 (Vehicles/Day)**	**Segment Crash Rate (Crashes per 100-Million Vehicle-Miles of Travel)**	**Wet-weather Segment Crash Rate (Crashes per 100-Million Vehicle-Miles of Travel)**
79.2	39.067017	-95.72994	363	0.29	4160	3497.653	1014.319
204.8	38.84885	-98.484	20	0.35	13500	59.38267	20.78393
214.7	38.99972	-96.86044	254	0.3	52800	192.825	57.84749
217.55	38.067623	-95.37895	16	0.38	62900	10.19607	3.874507
295.2	38.40518	-96.48997	9	0.22	26800	13.46081	2.961378
330.1	38.848427	-94.82388	73	0.42	5180	564.8805	237.2498
357.7	38.883774	-94.791336	825	0.28	57800	572.1232	160.1945

Table 17: Crash rates for clusters with more than 60 percent wet weather crashes that had more than 20 accidents during the study period.

Cluster ID Number	**Cluster Latitude**	**Cluster Longitude**	**Total Crashes in Cluster**	**Ratio of Accidents Occurring During Precipitation Event**	**Annual Average Daily Traffic as of 2021 (Vehicles/Day)**	**Segment Crash Rate (Crashes per 100-Million Vehicle-Miles of Travel)**	**Wet-weather Segment Crash Rate (Crashes per 100-Million Vehicle-Miles of Travel)**
7	37.76021	-97.00196	86	0.62	17400	198.1129	122.83
9	38.152863	-96.49227	24	0.62	16800	57.26186	35.50235
10	37.157745	-97.339455	28	0.61	19200	58.45481	35.65744
11	38.2322	-96.40461	43	0.65	16800	102.5942	66.6862
12	38.84987	-97.647125	44	0.61	21000	83.98406	51.23027
13	38.18108	-96.46171	55	0.76	16800	131.2251	99.73107
19	38.163666	-96.48202	28	0.68	16800	66.8055	45.42774

Crash rates can be compared from one location to another to identify where safety treatments can be considered. The locations with the highest crash rates were associated with clusters of high total crashes and low AADT volume. Although the number of accidents occurring during wet weather is lower than 60 percent for the KDOT locations, the cluster locations at RP 79.2 and the RP 330.1 experienced the highest crash rates and wet-weather crash rates when compared to the hot-spot clusters. Accounting for traffic using crash rates can be useful for deciding which location(s) should be corrected first for maximum benefit.

Chapter 4: Discussion and Conclusions

4.1 Summary

This research analyzed KDOT study locations to identify pavement performance during wet weather to assess possible hydroplaning shortcomings. To that end, it presented models and equations, discussed drainage and roadway texture, examined high friction surface treatments, exhibited data from site visits, and furnished ten years of Kansas highway crash data. It also explored ways to quantify and model water film thickness and hydroplaning and explored solutions for issues. Thereafter, it suggested future investigations for superelevated transition hydroplaning remediation. All information can be applied to current superelevated highway transition sites and to future highway designs which may need to consider roadway infrastructure vulnerability due to climate change and increased high wet weather frequency for Kansas drivers.

Sample locations identified by KDOT engineers were considered as areas for solution investigation. Using data that was freely available and tools that are openly available for highway design, the study locations were examined. A method of identifying where flow is likely to gather and the path it was likely to take was used by considering LCMS and LDTM data. MTD was also used to classify suitable pavement texture that could also impact the WFT on roadways that relates to hydroplaning. Future areas of investigation for remediation were made for the study locations based on these findings. Other that the RP 295.2 location, where a texture improvement investigation can be recommended, suggestions for drainage and geometry investigation improvements can be made for the majority of the KDOT study locations.

An example redesign of the RP 295.2 location experiencing unique results of flow direction and accumulation was considered. A method for a simple method for slope-flow-path minimization was suggested to achieve a reduction in the predicted length that flow would travel

on the designed roadway. For the example location selected, it was found that the longitudinal slope was adequate for drainage, and that a reconfiguration of the on-ramp could not be considered. Reducing the superelevated transition length resulted in shorter slope-flow-paths at the transition. In this example, the longer of the redesigned transitions resulted in shorter slope-flow-paths.

A broader impaction of hydroplaning in Kansas was also explored. Twenty-six crash clusters were identified as having a large portion of their crashes occurring during wet weather. Locations in Kansas where a wet-weather crashes occur more often was explored to address where hydroplaning was potentially more likely to occur. It was found that the clusters closest to the study locations experienced a lower percentage of crashes that occurred during precipitation events compared to clusters of the highest wet-weather crash percent. In relation to this, areas were compared using crash rates to identify which locations were more prone to wet-weather crashes based on traffic volumes. It was found that the cluster locations at RP 79.2 and the RP 330.1 experienced the highest crash rates and wet-weather crash rates when compared to all the locations explored. A change in climate would create more extreme weather events that would potentially worsen hydroplaning at the most susceptible locations. These most vulnerable locations should be considered for hydroplaning mitigation.

4.2 Uncertainty and Limitations

Proper pavement and roadway modeling is a limitation that can be discussed. Limitations identified in this area are be summarized below:

- Roadway meshes created as a means to investigate flow-path minimization are uniform and are completely flat geometry. This is unrealistic when considering the non-uniformity of a roadway as well as the microtexture and macrotexture of a roadway surface.

- Although reduced texture indicates road surface wear and can decrease the surface's ability to drain water, a proper study of roadway friction should be conducted before texture improvements should be made at the study locations.
- Porous pavements were not considered in this research. The models created in ORD and ArcGIS Pro do not allow for porous surfaces, which would impact the results of flow accumulation, flow direction, and slope path modeling.
- Digital "banding" of the digital terrain map scans would also impact the results of flow direction and accumulation results. An example of this can be seen in the eastern portion of the 330.1 location in Figure 36 and could reflect some amount of error associated with how LDTM and LCMS data was collected.
- LDTM and LCMS data was collected using longitudinal bands that may not represent the entirety of a roadway section.
- Multiple redesign solutions have to be compared when considering flow path minimization using slope paths as seen in ORD. As seen in the example shorter transition distances do not always result in shorter flow paths.

Although the method that was used for clustering crashes was broadly applicable to locations, the following limitations were identified involving the method of crash clustering that was explored:

- The accuracy of the crash reports is affected by time uncertainties, weather conditions, and crash locations. These variables impact the final accuracy of the clustering model, and a more in-depth crash cluster needs to be initiated to improve the results when estimating locations of high wet-weather crashes.

- Clusters of these crashes did not account for precipitation type, accident direction or lane, data accuracy, traffic amount, or roadway configuration, which could impact the results of crash clusters. Traffic volume for crash clusters was explored, but these areas could be related to where a higher rate of crashes occurs overall.
- The KDOT study areas that have been identified as having reports of hydroplaning were not identified using this clustering technique.
- Crashes that occurred during wet weather were assumed to have been caused by wet weather. Crashes caused by factors unrelated to hydroplaning (e.g., driver error, wildlife, roadway ice) were not filtered form the clustered crashes relating to wet weather.
- Clusters identified only locations where crashes had occurred. Areas of serious hydroplaning where no accidents had occurred were not recognized.
- Crashes could have unnecessarily been identified as wet-weather incidents with the use of a +/- 2-hour time span from the time of crash.
- Crashes were characterized as occurring during precipitation events using the NLDAS data set. There is some amount of error using this data set based on locations, precipitation types, and finding beginning and end times of precipitation events.

4.3 Future Work

Rainfall intensity is an area of hydroplaning that could be explored further in relation to crash location. Areas with high wet-weather crashes in relation to rainfall intensity such as in Singh Dhaliwal (2017) and Saberi and Bertini (2010) is a possible area of future work. Locations with lower rainfall intensities that result in wet-weather related crashes could be consider first for hydroplaning reduction projects. In relation to this, when suggesting improvements for certain

areas, further research can be conducted regarding surface texture and grooving. At locations of low texture, a rainfall intensity and resulting WFT on the roadway can be evaluated. Optimal texture when considering WFT can be researched, and different roadway surface texture types and grooving methods using varying roadway surface materials can be explored. Best practices for roadway texture and grooving concerning rain intensities can be researched and applied at a large scale if digital scans of roadway surfaces are available.

Another consideration for future research would be a methodology for highway redesign projects concerning drainage and geometry improvements. A step-by-step approach for highway redesign projects involving hydroplaning improvements would be beneficial for state DOTs. Additionally, universal guidelines can also be developed for when a section of roadway should be considered for a redesign improvement related to wet-weather crashes. For example, the 2023 FDOT highway design manual (McDaniel et al. 2022) suggests redesign improvements for wet weather based on the number of crashes a location experiences, but additional considerations can be made for areas of low texture and slope.

An expansion of identifying hydroplaning hotspots to investigate vulnerable roadways can be investigated. A state-wide project for identifying and assessing hydroplaning could recognize parameters like free flow time, congested flow time, roadway section length, assigned traffic volumes to roadway sections, isolating crashes to urban and rural settings at an exceptionally large scale, only clustering crashes in the same direction of travel, and limiting crashes to those only occurring during rain. A more refined clustering method considering more parameters can potentially better identify areas of wet-weather crashes. Being able to identify areas with wet-weather crashes using high accuracy will make the process of correcting the cause of the crashes

much easier. Better identification of areas of that have high hydroplaning potential is important for driver safety and roadway rehabilitation.

References

AASHTO. 2018. *A policy on geometric design of highways and streets, 2018*. Washington, DC: American Association of State Highway and Transportation Officials.

Anderson, D. A., R. S. Huebner, J. R. Reed, J. C. Warner, and J. J. Henry. 1998. "Improved Surface Drainage of Pavements." *NCHRP Web-Only Document*, (16).

Anselin, L. 1995. "Local Indicators of Spatial Association—LISA." *Geographical Analysis*, 27 (2): 93–115. https://doi.org/10.1111/j.1538-4632.1995.tb00338.x.

"ArcGIS Pro." 2022. Esri.

ASTM. 2019. *Standard Test Method for Measuring Pavement Macrotexture Depth Using a Volumetric Technique*. ASTM International.

Bill, A., D. A. Noyce, J. Yambo, H. Bahia, and J. Chapman. 2007. *Incorporating road safety into pavement management: maximizing surface friction for road safety improvements*. Technical Report. Midwest Regional University Transportation Center.

Boulet, M., G. Descornet, and J. C. Wambold. 1995. "International Experiment to Compare and Harmonize Skid Resistance and Texture Measurements." *Routes/Roads*, (288).

Brown, S. A., J. D. Schall, J. L. Morris, C. L. Doherty, S. M. Stein, and J. C. Warner. 2009. "Urban Drainage Design Manual Hydraulic Engineering Circular 22, Third Edition."

Browne, A. L. 1975. "Mathematical Analysis for Pneumatic Tire Hydroplaning." https://doi.org/10.1520/STP39045S.

Caltrans. 2020. "Highway Design Manual (HDM) | Caltrans." Accessed November 18, 2022. https://dot.ca.gov/programs/design/manual-highway-design-manual-hdm.

Chesterton, J., N. Nancekivell, and N. Tunnicliffe. 2006. "The use of the Gallaway formula for aquaplaning evaluation in New Zealand." *TRANSIT NEW ZEALAND AND NEW*

ZEALAND INSTITUTE OF HIGHWAY TECHNOLOGY (NZIHT) ANNUAL CONFERENCE, 8TH, 2006, AUCKLAND, NEW ZEALANN.

City of Lenexa. n.d. “Rehabilitation Techniques.” Accessed November 30, 2022. https://www.lenexa.com/government/departments___divisions/municipal_services/pavement_management_program/rehabilitation_techniques.

City of Salina. 2020. “City of Salina Pavement Management Street Maintenance Program.” Accessed November 30, 2022. http://www.salina-ks.gov/filestorage/18184/18599/20877/20979/Street_Maintenance_Presentation_10-29-20.pdf.

Dong, X., H. Guo, and S. Zeng. 2017. “Enhancing future resilience in urban drainage system: Green versus grey infrastructure.” *Water Res*, 124: 280–289. https://doi.org/10.1016/j.watres.2017.07.038.

Drenth, K. P., F. H. Ju, and J. Y. Tan. 2017. “Sampling functional condition indices at traffic-speed.” *Bearing Capacity of Roads, Railways and Airfields*. CRC Press.

Flintsch, G. W., J. B. Ferris, S. Taheri, S. Katicha, Y. Kang, A. Nazari, E. de Leon Izeppi, K. Velez, F. Battaglia, L. Chen, D. Kibler, K. K. McGhee, National Cooperative Highway Research Program, Transportation Research Board, and National Academies of Sciences, Engineering, and Medicine. 2021. *Guidance to Predict and Mitigate Dynamic Hydroplaning on Roadways*. 26287. Washington, D.C.: Transportation Research Board.

Gallaway, B. M., G. G. Hayes, D. L. Ivey, W. B. Ledbetter, and R. M. Olson. 1979. *Pavement and Geometric Design Criteria for Minimizing Hydroplaning. A Technical Summary.* Texas Transportation Inst., College Station.; Federal Highway Administration, Washington, DC.

Gallaway, B. M., R. E. Schiller, and J. G. Rose. 1971. “Effects of Rainfall Intensity, Pavement Cross Slope, Surface Texture, and Drainage Length on Pavement Water Depths.” 86.

Golembiewski, G., and B. Chandler. 2011. *Roadway Departure Safety: A Manual for Local Rural Road Owners*. FHWA.

Gunaratne, M., Q. Lu, J. Yang, W. Jayasooriya, M. Yassin, S. Amarasiri, and University of South Florida. Dept. of Civil and Environmental Engineering. 2012. *Hydroplaning on multi lane facilities.*

Gurganusa, C. F., S. Chang, and N. G. Gharaibeh. 2021. “Evaluation of hydroplaning potential using Mobile Lidar measurements for network-level pavement management applications.” *Road Materials and Pavement Design*, 23 (6): 1390–1399. Taylor & Francis. https://doi.org/10.1080/14680629.2021.1899962.

Hall, J. W., K. L. Smith, P. Littleton, Transportation Research Board, National Cooperative Highway Research Program, and Transportation Research Board. 2009. *Texturing of Concrete Pavements*. 14318. Washington, D.C.: National Academies Press.

Henry, J. J. 2000. “Evaluation of Pavement Friction Characteristics.” *NCHRP Synthesis of Highway Practice*, (291).

Hibbs, B. O., and R. M. Larson. 1996. *Tire Pavement Noise and Safety Performance, PCC Surface Texture Technical Working Group*.

Holgado-Barco, A., D. Gonzalez-Aguilera, P. Arias-Sanchez, and J. Martinez-Sanchez. 2014. “An automated approach to vertical road characterisation using mobile LiDAR systems: Longitudinal profiles and cross-sections.” *ISPRS Journal of Photogrammetry and Remote Sensing*, 96: 28–37. https://doi.org/10.1016/j.isprsjprs.2014.06.017.

Iowa DOT. 2019. “Superelevation Transition Evaluation Tool.” 3.

Jayasooriya, W., and M. Gunaratne. 2014. “Evaluation of Widely used Hydroplaning Risk Prediction Methods using Florida’s past Crash Data.” *Transportation Research Record*, 2457 (1): 140–150. SAGE Publications Inc. https://doi.org/10.3141/2457-15.

Jeong, J., and R. J. Charbeneau. 2010. “Diffusion Wave Model for Simulating Storm-Water Runoff on Highway Pavement Surfaces at Superelevation Transition.” *Journal of Hydraulic Engineering*, 136 (10): 770–778. American Society of Civil Engineers. https://doi.org/10.1061/(ASCE)HY.1943-7900.0000253.

KDOT. 2014a. “Design Manual.” Volume I.

KDOT. 2014b. “KDOT: Traffic Count Maps.” *Default-Template*. page. Accessed August 26, 2022. https://www.ksdot.org/burtransplan/maps/mapstrafficdist.asp.

KDOT. 2017. “Crash Data Unit.” page. Accessed November 26, 2022. https://www.ksdot.org/bureaus/burTrafficSaf/CrashDataUnit.asp.

KDOT. 2019. *State of Kansas Law Enforcement Crash Report Coding Manual*.

KDOT. 2022. “2021 KDOT MOBILE LiDAR PROJECT DATA PORTAL.” *Kansas Department of Transportation*. page. Accessed November 17, 2022. https://www.ksdot.org/bureaus/burTransPlan/Lidar/home.asp.

Kummer, H. W., and W. E. Meyer. 1963. “The Penn State Road Friction Tester as Adapted to Routine Measurement of Pavement Skid Resistance.” 31.

“LAStools.” 2021. rapidlasso GmbH.

Laurent, J., D. Lefebvre, and E. Samson. 2008. “Development of a new 3D transverse laser profiling system for the automatic measurement of road cracks.”

Ledl, T. 2004. “Kernel Density Estimation: Theory and Application in Discriminant Analysis.” *Austrian Journal of Statistics*, 33 (3): 267–279. https://doi.org/10.17713/ajs.v33i3.441.

Lee, H., and D. Ayyala. 2020. *Enhanced Hydroplaning Prediction Tool*.

Li, P., C. Sun, M. Huang, S. Jiang, and M. D. Khan. 2022. "Water accumulation and anti-sliding decay characteristics of freeway pavement at superelevation transitions." *Road Materials and Pavement Design*, 1–16. https://doi.org/10.1080/14680629.2022.2106294.

Lottes, S. A., M. A. Sitek, and N. Sinha. 2020. *Computational Analysis of Water Film Thickness During Rain Events for Assessing Hydroplaning Risk, Part 1: Nearly Smooth Road Surfaces*. Argonne National Lab. (ANL), Argonne, IL (United States).

Martinez, J. E., R. D. Young, and W. C. Faatz. 1976. "Effects of Pavement Grooving on Friction, Braking, and Vehicle Control." 192.

Mattioli, G., C. Roberts, J. K. Steinberger, and A. Brown. 2020. "The political economy of car dependence: A systems of provision approach." *Energy Research & Social Science*, 66: 101486. https://doi.org/10.1016/j.erss.2020.101486.

McDaniel, G., D. Amato, D. Carver, D. Lewis, B. Gerrell, J. Morris, and T. Gehrke. 2022. *2023 FDOT Design Manual*. 1257.

Merritt, D., S. Himes, and R. J. Porter. 2021. *High Friction Surface Treatment Site Selection and Installation Guide*. 144.

Merritt, D., C. Lyon, and B. Persaud. 2015. *Evaluation of Pavement Safety Performance*.

"NLDAS: Project Goals." 2022. *NLDAS: Project Goals*. Accessed December 1, 2022. https://ldas.gsfc.nasa.gov/nldas.

Noureldin, A. S., S. Li, K. Zhu, and Y. Jiang. 2006. "Surface Friction on Longitudinally Tined Concrete Pavements: New Findings from Field Testing and Finite-Element Analysis Simulation."

OECD. 2018. “Climate-resilient Infrastructure.” Accessed December 1, 2022. https://www.oecd.org/environment/cc/policy-perspectives-climate-resilient-infrastructure.pdf.

Ong, G. P., and T. F. Fwa. 2007. “Wet-Pavement Hydroplaning Risk and Skid Resistance: Modeling.” *Journal of Transportation Engineering*, 133 (10): 590–598. American Society of Civil Engineers. https://doi.org/10.1061/(ASCE)0733-947X(2007)133:10(590).

Ong, G. P., T. F. Fwa, and J. Guo. 2005. “Modeling Hydroplaning and Effects of Pavement Microtexture.” *Transportation Research Record*, 1905 (1): 166–176. SAGE Publications Inc. https://doi.org/10.1177/0361198105190500118.

“OpenRoads Designer: Road Design Software | Bentley Systems.” 2022. Accessed December 16, 2022. https://www.bentley.com/software/openroads-designer/.

“Pavemetrics | Laser Crack Measurement System (LCMS).” n.d. *Pavemetrics*. Accessed November 24, 2022. https://www.pavemetrics.com/applications/road-inspection/lcms2-en/.

“Pavemetrics | Laser Digital Terrain Mapping System (LDTM).” n.d. *Pavemetrics*. Accessed November 24, 2022. https://www.pavemetrics.com/applications/digital-terrain-mapping/laser-digital-terrain-mapping-system/.

Pourhassan, A., A. A. Gheni, and M. A. ElGawady. 2022. “Water Film Depth Prediction Model for Highly Textured Pavement Surface Drainage.” *Transportation Research Record*, 2676 (2): 100–117. SAGE Publications Inc. https://doi.org/10.1177/03611981211036349.

Pranjić, I., and A. Deluka-Tibljaš. 2022. “Pavement Texture–Friction Relationship Establishment via Image Analysis Methods.” *Materials (Basel)*, 15 (3): 846. https://doi.org/10.3390/ma15030846.

Rajaei, S., K. Chatti, and R. Dargazany. 2017. “A Review: Pavement Surface Micro-texture and Its Contribution to Surface Friction.”

Ross, N., and K. Russam. 1968. “THE DEPTH OF RAIN WATER ON ROAD SURFACES.”

Saberi, M., and R. L. Bertini. 2010. “Empirical Analysis of the Effects of Rain on Measured Freeway Traffic Parameters.”

Shams, A., W. A. Sarasua, A. Famili, W. J. Davis, J. H. Ogle, L. Cassule, and A. Mammadrahimli. 2018. “Highway Cross-Slope Measurement using Mobile LiDAR.” *Transportation Research Record*, 2672 (39): 88–97. SAGE Publications Inc. https://doi.org/10.1177/0361198118756371.

Singh Dhaliwal, S. 2017. “The Effects of Rain on Freeway Traffic in Southern California.” California State Polytechnic University, Pomona.

Sitek, M., and S. Lottes. 2020. *Computational Analysis of Water Film Thickness During Rain Events for Assessing Hydroplaning Risk Part 2: Rough Road Surfaces*. ANL--20/37, 1677647, 162561.

Snyder, M. 2019. *Concrete Pavement Texturing*. 17.

Snyder, M. B. 2006. *Pavement Surface Characteristics: A Synthesis and Guide*.

Souleyrette, R., S. Hallmark, S. Pattnaik, M. O’Brien, and D. Veneziano. 2003. “Grade and Cross Slope Estimation from LIDARbased Surface Models.”

Trenberth, K. E. 2011. “Changes in precipitation with climate change.” *Climate Research*, 47 (1–2): 123–138. https://doi.org/10.3354/cr00953.

Tsai, Y. (James), C. Ai, Z. Wang, and E. Pitts. 2013. “Mobile Cross-Slope Measurement Method Using Lidar Technology.” *Transportation Research Record*, 2367 (1): 53–59. SAGE Publications Inc. https://doi.org/10.3141/2367-06.

Xia, Y., K. Mitchell, M. Ek, J. Sheffield, B. Cosgrove, E. Wood, L. Luo, C. Alonge, H. Wei, J. Meng, B. Livneh, D. Lettenmaier, V. Koren, Q. Duan, K. Mo, Y. Fan, and D. Mocko. 2012. “Continental-scale water and energy flux analysis and validation for the North American Land Data Assimilation System project phase 2 (NLDAS-2): 1. Intercomparison and application of model products.” *Journal of Geophysical Research: Atmospheres*, 117 (D3). https://doi.org/10.1029/2011JD016048.

Yamada, I., and J.-C. Thill. 2004. “Comparison of planar and network K-functions in traffic accident analysis.” *Journal of Transport Geography*, 12 (2): 149–158. https://doi.org/10.1016/j.jtrangeo.2003.10.006.

Zahir, H., S. Islam, M. Hossain, and Kansas State University. Transportation Center. 2017. *Friction management on Kansas Department of Transportation highways.*

Zhang, K., and H. C. Frey. 2006. “Road Grade Estimation for On-Road Vehicle Emissions Modeling Using Light Detection and Ranging Data.” *Journal of the Air & Waste Management Association*, 56 (6): 777–788. Taylor & Francis. https://doi.org/10.1080/10473289.2006.10464500.

Zuniga-Garcia, N., and J. A. Prozzi. 2019. “High-Definition Field Texture Measurements for Predicting Pavement Friction.” *Transportation Research Record*, 2673 (1): 246–260. SAGE Publications Inc. https://doi.org/10.1177/0361198118821598.